remote sensing

MDPI

Article

Feasibility Study of Tractor-Test Vehicle Technique for Practical Structural Condition Assessment of Beam-Like Bridge Deck

Yang Yang [1,*], Quan Cheng [1], Yuanhao Zhu [1], Lilei Wang [1] and Ruoyu Jin [2]

[1] MOE Key Laboratory of New Technology for Construction of Cities in Mountain Area and School of Civil Engineering, Chongqing University, Chongqing 400044, China; 201716021035@cqu.edu.cn (Q.C.); 201716131147@cqu.edu.cn (Y.Z.); 20161602012t@cqu.edu.cn (L.W.)

[2] Subject of Built Environment, School of Environment and Technology, University of Brighton, Brighton 02215, UK; R.Jin@brighton.ac.uk

* Correspondence: yangyangcqu@cqu.edu.cn; Tel: +86-18680849683

Received: 6 November 2019; Accepted: 22 December 2019; Published: 1 January 2020

Abstract: The tractor-test vehicle technique of non-destructive testing for indirect measurement of the modal properties of a bridge deck is revisited in this paper with several improvements for possible practical application to the structural condition assessment of a beam-like bridge deck. The effect of damping of the vehicle-bridge system is considered and the modal properties from only the first vibration mode of the structure will be used for a quick and simple assessment. The two test vehicles are designed to have the same modal frequency and damping ratio but with parameters in the follower No.2 test vehicle proportional to those in the follower No.1 test vehicle. This effectively removes the effect of road surface roughness in the response of an equivalent vehicle such that the error in the subsequent condition assessment is reduced. Through data collected on-sitetransmitted to theremote computer platform, a simple technique based on the moment-curvature relationship acceptable to practical engineers is adopted for the condition assessment with improvements in the estimation of the element bending stiffness of the deck. Scenarios with different damping, vehicle speed, road surface roughness, and local damages in the bridge structure are studied with or without temperature effect in the measurement. Through numerical simulations and field tests, the tractor-test vehicle technique of non-destructive testing with the proposed modifications and improvements has been demonstrated to give consistently accurate estimates of the element bending stiffness of the bridge deck but with a small error close to the end of the deck.

Keywords:tractor-test vehicle technique; bridge deck; assessment; element bending stiffness; damping; vehicle speed; road surface roughness; temperature

1. Introduction

Conventionally, system identification of bridge structures in non-destructive testing is based on measured responses of the structure [1], therefore, the sensor must be mounted directly on the bridge deck such as the Golden Gate Bridge and Tsing Ma Bridge [2,3]. However, this approach suffers from the drawback of a large capital cost as well as the closure of the bridge. In addition, the massive data monitored by the sensors is difficult to process effectively [4]. All these characteristics have limited the application and promotion of direct measurement methods in bridge health monitoring.

Due to the above drawbacks in the direct measurement of non-destructive testing method, advantage has been taken with a coupled system where the modal frequencies of a bridge deck has been successfully estimated [5,6] and verified immediately in the field test [6,7] from the responses of a passing vehicle and improvements in the resolution and reliability of the method. The mode shapes of the bridge deck were also constructed from the responses of the moving vehicle [8,9] using

the instantaneous amplitude or Hilbert transformation. Malekjafarian and Obrien [10,11] proposed the Short Time Frequency Domain Decomposition method to identify bridge mode shapes from the responses of two identical following vehicles, which is not a single degree of freedom system for the following vehicles with four wheels in each vehicle. Other researchers have used measured data from both the bridge deck and [12] an instrumented vehicle for the identification of natural frequencies of the structure. Kim and Lynch [13] used the synchronized responses from wireless sensors installed on the bridge and the moving vehicle to study their dynamic interaction. The fundamental frequency of a bridge obtained from the vibration response of an instrumented two-axle vehicle was also studied [14]. Based on the model of a single vehicle passing through a two-span continuous beam bridge, Sitton et al. [15] derived a closed solution for the vehicle response, theoretically analyzed the bridge frequency components contained in the vehicle response, and verified the theoretical solution by numerical simulation. Gonzalez et al. [16] proposed a method for identifying the damping of a bridge structure using a moving vehicle. OBrien and co-workers [17] proposed a method to detect changes in the damping of a bridge with a truck–trailer vehicle system. Yang et al. [18] proposed a method for identifying the damping ratios of simply supported beams using a two-axle moving test vehicle, equipped with uniformly spaced accelerometers and laser sensors in an ideal model.

Road roughness is a factor that needs to be considered when applying the indirect measurement of non-destructive testing to practice because it often has a direct negative effect on the identification of the bridge modal properties as mentioned above. K.C. Chang et al. [19]'s research shows that the surface roughness of the bridge has an adverse effect on the extraction of bridge frequencies, and the mode shapes obtained were approximate due to the averaging process of the method with consideration of good road surface roughness without details of mechanics derivation. Yang et al. [20] proposed the use of two connected vehicles to indirectly measure the bridge frequencies with the removal of the effect of road surface roughness without considering damping for both the vehicles and bridge. Kong et al. [21] used a test vehicle consisting of a tractor and two following identical trailers to estimate the bridge mode shape from the vehicle responses based on the single vehicle-bridge couple system. However, it does not consider the damping of the vehicles and the bridge and their coupling, and the corresponding damage identification is even more difficult to refer.

The indirect approach of non-destructive testing has been applied to study various problems in bridge engineering. The measured response of a moving vehicle over a bridge deck was also used for the damage assessment of the structure [22] subjected to the effects of small road surface roughness. Kim and Kawatani [23] also conducted the damage detection of a bridge deck considering the effects of vehicle-bridge coupling and the road surface roughness. The tension loss in cables and local damages in a cable-stayed bridge were also estimated from responses of a moving vehicle [24]. Lu and Liu [25] numerically identified the bridge local damages and vehicle parameters based on the response sensitivity analysis on the dynamic response of both the bridge and the passing vehicle. Miyamoto and Yabe [26] conducted studies on assessing the condition of existing short span and medium-span reinforced prestressed concrete bridges based on vibration monitoring data obtained from the in-service public bus equipped with vibration measurement instrumentations. Zhang et al. [27,28] developed a damage detection method based on the squares of the approximately extracted structural mode shapes from the acceleration of a passing tapping vehicle and a method based on the curvature of the operating deflection shape. Li and Au [29] performed the damage detection of bridges with road surface roughness using the response of a moving vehicle. Feng and Feng [30] conducted an output-only damage detection of bridges using the vehicle-induced displacement response and mode shape curvature index. Based on the vehicle bridge coupling model, Mei et al. [31] used mel-frequency cepstral coefficients and principal component analysis to identify the damage and damage severity of the bridge and verified the method by numerical simulation. Yang et al. [32] proposed a bending mode recognition based on the frequency domain and an optimization algorithm based on the time domain to identify bridge damage through vehicle response, however the influence of road surface roughness is not considered in the numerical simulation. The above research on damage identification has just started on the preliminary step, and no practical damage

indicators based on indirect measurement have been proposed. Further the lack of further verification of the proposed method by the field bridge test.

Various indices have been proposed for damage detection of structures in direct measurement for non-destructive testing. Modal strain energy has been proposed by Shi et al. [33] to locate and quantify local damages in a two-story steel portal frame. Kim et al. [34] compared the crack detection of gusset plates using various indices, and they found that parameters such as mode shapes, flexibility, frequency response functions, and curvatures are sensitive to small perturbations. The damage identification conducted by Li et al. [35] was based on the minimization of the difference between the measured and reconstructed response vectors from acceleration responses of the damaged substructure. The response reconstruction is based on transforming the measured responses into responses at selected locations with the transmission matrix. Zhong and Yang [36] used the mode shape curvatures before and after damage occurs to identify the damage locations and severity of plate-like structures. Samami and Oyadiji [37] employed the analytical and numerical curvatures to generate modal displacement of a damaged beam with very small crack-like surface flaws or open slots for the development of a damage detection method. Yang et al. [38] proposed a fusion of statistical moments by combining the fourth-order statistical moment of displacement with the eighth-order statistical moment of acceleration for the damage identification of structures. OBrien et al. [39] presented an optimal parameter of the least square method for identifying the interaction forces and corresponding global bending stiffness through the response of the half-car model moving over the bridge. Other problems such as the effect of uncertainties in the environment, nonlinear damage process, as well as the optimal locations of sensors and noise contamination in measurement, should all be considered in the selection of damage indices for the structural damage detection [40,41].

Different from the overall bending stiffness identification of one span in the former research [42], element flexural stiffness can be regarded as the damage index, it can directly represent damage and has a clear physical meaning. Based on the element bending stiffness, the deformation deflection of multiple bridge sections under arbitrary loads can be calculated. The direct stiffness calculation (DSC) [43,44] was originally proposed for the calculation of each element flexural stiffness of a simply-supported beam using the moment-curvature relationship. The modal curvatures were determined by a penalty-based smoothing procedure, where the objective function was formulated as the difference between the approximated and measured displacement mode shape with compatibility requirements [45]. The penalty factors, however, need to be carefully chosen, and they are generally dependent on the damage locations [46]. An improved DSC method was proposed [47] to remove this limitation. The modal curvatures were calculated directly from the measured displacement mode shapes with the central difference method. Based on the sensitivity of identified modal parameters and the study of measurement noise to different mode shapes, it was shown effective in the numerical and experimental damage detection of continuous and simply-supported beams [1,45]. The improved DSC was further validated in the damage detection of a 12-story reinforced concrete frame structure under the shaking table test [47]. It is, however, noted that the identification results near the simply-supported end of beams or bridge abutments are not good due to the difficulty in estimating curvatures at these locations.

Some scholars have published the use of two following normal vehicles [10,11] and two single-axle vehicles [20,21] going across the bridge at once with the indirect method to remove the road surface roughness effect. This paper reports on the feasibility of the tractor-test vehicle technique (TTVT) for a quick and practical assessment of beam-like structures based on the identified element bending stiffness. This paper describes a general configuration consisting of two test vehicles of different masses and tractor, in which only two test vehicles are required to have the same modal frequency and damping ratio, but not the same vehicle, and each test vehicle going across the bridge separately. It corrects the contradiction between the theory of a single axle coupling system and the numerical simulation of multiple vehicles[21]. Considering different ways of former operation [10,11,20,21], i.e., two single test vehicles with the same tractor going across the bridge at a time in the former way, this case is two single vehicles going across the bridge respectively, therefore, there

are two crossing bridges; and the details of theory derivation with coupling in tractor, test vehicle, and bridge system for non-destructive testing are demonstrated, which is coordinated with numerical simulation and field test. The TTVT of non-destructive testing was also improved with consideration of damping and non-uniform speed of the vehicle-bridge system and environmental temperature. The improved DSC method was further improved to obtain accurate bridge element bending stiffness for damage identification. The modified TTVT was finally studied for its feasibility in field application.

This paper starts with a brief introduction of the basic concept of the TTVT followed by the presentation of the improvements made to existing techniques, i.e., obtaining the bridge frequency and mode shape from the indirect measurement signal of test vehicles responses; and then the bridge bending stiffness of each element can be calculated. Theory derivation of the TTVT based on vehicle-bridge couple system of non-destructive testing on mechanics is explained. The analysis procedure is then given. Numerical simulations on the effect of different influential factors are conducted to study the potential problems involved with the field test application. Then, the proposed method is preliminarily verified by a field test.Finally, conclusionsare drawn on the benefits and weaknesses of the proposed method that need further research for non-destructive testing.

2. The Tractor-Test Vehicle Technique (TTVT) of Non-Destructive Testing

The entire non-destructive testing based on the TTVT is included in the following part:

2.1. Indirect Measurement of Mode Shape of Bridge Structures

In Figure 1, a test vehicle (No.1 or No.2 test vehiclewill be mentioned in the following research)and a tractor with a distance spacing of $\Delta L$are moving on a bridge deck at a constant speed v. The tractorandthe test vehicle are simplified as a moving sprung mass $m_{v,2}$ and $m_{v,1}$, supported on a dashpot of damping coefficient c_{v2}, c_{v1} and a spring of stiffness k_{v2}, and k_{v1}, respectively. The bridge is simply-supported with length L, mass m^* per unit length, and bending stiffness EI with a damping ratio of the n^{th}mode ξ_n , there the bending stiffness EI here includes the contribution of non-structural members such as bridge railings and bridge deck pavements in actual bridges, and the mass per unit length m^* can be obtained from the actual bridge design data or preliminary estimated by the area of cross-section. The bridge is assumed at rest prior to the arrival of the test vehicle.

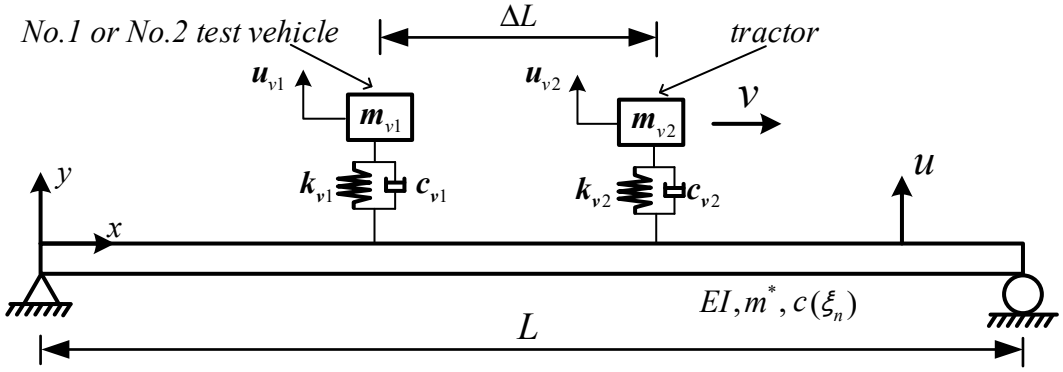

Figure 1. Spring mass moving over a bridge.

The equations of motion of the test vehicle, tractor, and bridge can be written as:

$$m_{v,1}\ddot{u}_{v1}(t)+k_{v1}(u_{v1}(t)-u(x,t)\big|_{x=vt})+c_{v1}(\dot{u}_{v1}(t)-\dot{u}(x,t)\big|_{x=vt})=0 \tag{1}$$

$$m_{v,2}\ddot{u}_{v2}(t)+k_{v2}(u_{v2}(t)-u(x,t)\big|_{x=vt_a})+c_{v2}(\dot{u}_{v2}(t)-\dot{u}(x,t)\big|_{x=vt_a})=0 \tag{2}$$

$$m^*\ddot{u}(x,t)+c\dot{u}(x,t)+EIu''''(x,t)=f_{c1}(t)\delta(x-vt)+f_{c2}(t)\delta(x-vt_a) \tag{3}$$

where $u(x,t)$ denotes the vertical displacement of the bridge structure at distance x from the left support and time t, $u_{v1}(t), u_{v2}(t)$ is the vertical displacement of the test vehicle and tractor respectively, measured from its static equilibrium position. $\dot{u}_{v1}(t), \dot{u}_{v2}(t)$ and $\dot{u}(x,t)$ indicatederivatives, partial derivatives of $u_{v1}(t), u_{v2}(t)$ and $u(x,t)$ with respect to time respectively. $\ddot{u}_{v1}(t), \ddot{u}_{v2}(t)$ and $\ddot{u}(x,t)$ indicate second-order time derivatives and time spatial derivative for the vertical displacement of the vehicle and the vertical displacement of the bridge,respectively. $u''''(x,t)$ indicatesa fourth-order spatial derivative of the vertical displacement of the bridge $u(x,t)$. It should be noted that the time t refers to the time after the test vehicleenters the bridge, so the equivalent time of the tractor relative to the test vehicle is $t_a = t + \Delta L / v = t + t_s$. When $x = vt$ and $x = vt_a$, the interaction force $f_{c1}(t), f_{c2}(t)$ at the contacts point of the test vehicle and tractor with the deck may be written as respectively,

$$f_{c1}(t) = -m_{v,1}g + k_{v1}(u_{v1}(t) - u(x,t)\big|_{x=vt}) + c_{v1}(\dot{u}_{v1}(t) - \dot{u}(x,t)\big|_{x=vt}) \tag{4}$$

$$f_{c2}(t) = -m_{v,2}g + k_{v2}(u_{v2}(t) - u(x,t)\big|_{x=vt_a}) + c_{v2}(\dot{u}_{v2}(t) - \dot{u}(x,t)\big|_{x=vt_a}) \tag{5}$$

where g is the acceleration of gravity.

The vertical displacement of the bridge structure, $u(x,t)$, can be expressed in terms of the generalized coordinates $q_n(t)$ and the modal shapes, which are $\sin(n\pi x / L)$ for a simply supported beam:

$$u(x,t) = \sum_{n=1}^{\infty} \sin\frac{n\pi x}{L} q_n(t) \tag{6}$$

Assuming the vehicle mass m_{v1}, m_{v2} is much less than that of the deck, i.e., $m_{v1} \ll m^* L$ and $m_{v2} \ll m^* L$. This assumption is easy to implement for actual bridges. By substituting Equation (6) into Equation (3), multiplying by $\sin(n\pi x / L)$, integrating x from 0 to L, and according to the orthogonal conditions of the sinusoidal function, the n^{th} modal equation of equilibrium of the structure can be written as:

$$\ddot{q}_n(t) + 2\xi_n\omega_n\dot{q}_n(t) + \omega_n^2 q_n(t) = \left(-\frac{2m_{v,1}g}{m^* L}\right)\sin\frac{n\pi vt}{L} + \left(-\frac{2m_{v,2}g}{m^* L}\right)\sin\frac{n\pi vt_a}{L} \tag{7}$$

where ω_n is the n^{th} modal angular frequency of bridge vibration, given by:

$$\omega_n = \frac{n^2\pi^2}{L^2}\sqrt{\frac{EI}{m^*}} \tag{8}$$

For zero initial conditions, one can obtain the generalized coordinate $q_n(t)$ of the bridge from Equation (7) as:

$$
\begin{aligned}
q_n(t) = e^{-\xi_n\omega_n t}\Bigg\{ & -\frac{2m_{v,1}gL^3}{n^4\pi^4 EI}\times\frac{2\xi_n(n\pi v/L\omega_n)\cos\omega_n\sqrt{1-\xi_n^2}t}{[1-(n\pi v/L\omega_n)^2]^2+[2\xi_n(n\pi v/L\omega_n)]^2} \\
& -\frac{2m_{v,1}gL^3}{n^4\pi^4 EI}\times\frac{[2\xi_n^2-1+(n\pi v/L\omega_n)^2]}{[1-(n\pi v/L\omega_n)^2]^2+[2\xi_n(n\pi v/L\omega_n)]^2}\times\frac{n\pi v\sin\omega_n\sqrt{1-\xi_n^2}t}{L\omega_n\sqrt{1-\xi_n^2}}\Bigg\} \\
& -\frac{2m_{v,1}gL^3}{n^4\pi^4 EI}\times\frac{1-(n\pi v/L\omega_n)^2}{[1-(n\pi v/L\omega_n)^2]^2+[2\xi_n(n\pi v/L\omega_n)]^2}\times\sin\frac{n\pi v}{L}t \\
& -\frac{2m_{v,1}gL^3}{n^4\pi^4 EI}\times\frac{-2\xi_n(n\pi v/L\omega_n)}{[1-(n\pi v/L\omega_n)^2]^2+[2\xi_n(n\pi v/L\omega_n)]^2}\times\cos\frac{n\pi vt}{L} \\
& +e^{-\xi_n\omega_n t}\Bigg\{ -\frac{2m_{v,2}gL^3}{n^4\pi^4 EI}\times\frac{2\xi_n(n\pi v/L\omega_n)\cos\omega_n\sqrt{1-\xi_n^2}t}{[1-(n\pi v/L\omega_n)^2]^2+[2\xi_n(n\pi v/L\omega_n)]^2} \\
& -\frac{2m_{v,2}gL^3}{n^4\pi^4 EI}\times\frac{[2\xi_n^2-1+(n\pi v/L\omega_n)^2]}{[1-(n\pi v/L\omega_n)^2]^2+[2\xi_n(n\pi v/L\omega_n)]^2}\times\frac{\sin\omega_n\sqrt{1-\xi_n^2}t}{\omega_n\sqrt{1-\xi_n^2}}\Bigg\}\times\cos\frac{n\pi vt_s}{L} \\
& -\frac{2m_{v,2}gL^3}{n^4\pi^4 EI}\times\frac{1-(n\pi v/L\omega_n)^2}{[1-(n\pi v/L\omega_n)^2]^2+[2\xi_n(n\pi v/L\omega_n)]^2}\times\cos\frac{n\pi vt_s}{L}\times\sin\frac{n\pi v}{L}t \\
& -\frac{2m_{v,2}gL^3}{n^4\pi^4 EI}\times\frac{-2\xi_n(n\pi v/L\omega_n)}{[1-(n\pi v/L\omega_n)^2]^2+[2\xi_n(n\pi v/L\omega_n)]^2}\times\cos\frac{n\pi vt_s}{L}\times\cos\frac{n\pi v}{L}t \\
& +e^{-\xi_n\omega_n t}\Bigg\{ -\frac{2m_{v,2}gL^3}{n^4\pi^4 EI}\times\frac{((n\pi v/L\omega_n)^2-1)\cos\omega_n\sqrt{1-\xi_n^2}t}{[1-(n\pi v/L\omega_n)^2]^2+[2\xi_n(n\pi v/L\omega_n)]^2} \\
& -\frac{2m_{v,2}gL^3}{n^4\pi^4 EI}\times\frac{\xi_n\omega_n[(n\pi v/L\omega_n)^2-1]-2\xi_n(n\pi v/L\omega_n)\times n\pi v/L}{[1-(n\pi v/L\omega_n)^2]^2+[2\xi_n(n\pi v/L\omega_n)]^2}\times\frac{\sin\omega_n\sqrt{1-\xi_n^2}t}{\omega_n\sqrt{1-\xi_n^2}}\Bigg\}\times\sin\frac{n\pi vt_s}{L} \\
& -\frac{2m_{v,2}gL^3}{n^4\pi^4 EI}\times\frac{2\xi_n(n\pi v/L\omega_n)}{[1-(n\pi v/L\omega_n)^2]^2+[2\xi_n(n\pi v/L\omega_n)]^2}\times\sin\frac{n\pi vt_s}{L}\times\sin\frac{n\pi v}{L}t \\
& -\frac{2m_{v,2}gL^3}{n^4\pi^4 EI}\times\frac{1-(n\pi v/L\omega_n)^2}{[1-(n\pi v/L\omega_n)^2]^2+[2\xi_n(n\pi v/L\omega_n)]^2}\times\sin\frac{n\pi vt_s}{L}\times\cos\frac{n\pi v}{L}t
\end{aligned}
\tag{9}
$$

Substituting Equation (9) into Equation (6) then yields the vertical displacement of vehicle bridge contact as:

$$
\begin{aligned}
u(vt,t) = \sum_{n=1}^{\infty}\Bigg[& -\frac{m_{v,1}gL^3}{n^4\pi^4 EI}\times\frac{-2\xi_n(n\pi v/L\omega_n)}{[1-(n\pi v/L\omega_n)^2]^2+[2\xi_n(n\pi v/L\omega_n)]^2}-\frac{m_{v,2}gL^3}{n^4\pi^4 EI}\times\cos\frac{n\pi vt_s}{L}\times\frac{-2\xi_n(n\pi v/L\omega_n)}{[1-(n\pi v/L\omega_n)^2]^2+[2\xi_n(n\pi v/L\omega_n)]^2} \\
& -\frac{m_{v,2}gL^3}{n^4\pi^4 EI}\times\sin\frac{n\pi vt_s}{L}\times\frac{1-(n\pi v/L\omega_n)^2}{[1-(n\pi v/L\omega_n)^2]^2+[2\xi_n(n\pi v/L\omega_n)]^2}\Bigg]\times\sin\frac{2n\pi v}{L}t \\
& +\sum_{n=1}^{\infty}\Bigg[-\frac{m_{v,1}gL^3}{n^4\pi^4 EI}\times\frac{1-(n\pi v/L\omega_n)^2}{[1-(n\pi v/L\omega_n)^2]^2+[2\xi_n(n\pi v/L\omega_n)]^2}-\frac{m_{v,2}gL^3}{n^4\pi^4 EI}\times\cos\frac{n\pi vt_s}{L}\times\frac{1-(n\pi v/L\omega_n)^2}{[1-(n\pi v/L\omega_n)^2]^2+[2\xi_n(n\pi v/L\omega_n)]^2} \\
& -\frac{m_{v,2}gL^3}{n^4\pi^4 EI}\times\sin\frac{n\pi vt_s}{L}\times\frac{2\xi_n(n\pi v/L\omega_n)}{[1-(n\pi v/L\omega_n)^2]^2+[2\xi_n(n\pi v/L\omega_n)]^2}\Bigg]\times\left(1-\cos\frac{2n\pi v}{L}t\right) \\
& +\sum_{n=1}^{\infty}e^{-\xi_n\omega_n t}\times\Bigg[-\frac{m_{v,1}gL^3}{n^4\pi^4 EI}\times\frac{[2\xi_n^2-1+(n\pi v/L\omega_n)^2]}{[1-(n\pi v/L\omega_n)^2]^2+[2\xi_n(n\pi v/L\omega_n)]^2}\times\frac{n\pi v\sin\omega_n\sqrt{1-\xi_n^2}t}{L\omega_n\sqrt{1-\xi_n^2}} \\
& -\frac{m_{v,2}gL^3}{n^4\pi^4 EI}\times\cos\frac{n\pi vt_s}{L}\times\frac{[2\xi_n^2-1+(n\pi v/L\omega_n)^2]}{[1-(n\pi v/L\omega_n)^2]^2+[2\xi_n(n\pi v/L\omega_n)]^2}\times\frac{\sin\omega_n\sqrt{1-\xi_n^2}t}{\omega_n\sqrt{1-\xi_n^2}} \\
& -\frac{m_{v,2}gL^3}{n^4\pi^4 EI}\times\sin\frac{n\pi vt_s}{L}\times\frac{\xi_n\omega_n[(n\pi v/L\omega_n)^2-1]-2\xi_n(n\pi v/L\omega_n)\times n\pi v/L}{[1-(n\pi v/L\omega_n)^2]^2+[2\xi_n(n\pi v/L\omega_n)]^2}\times\frac{1}{\omega_n\sqrt{1-\xi_n^2}}\Bigg] \\
& \times[\cos\left(\omega_n\sqrt{1-\xi_n^2}-\frac{n\pi v}{L}\right)t-\cos\left(\omega_n\sqrt{1-\xi_n^2}+\frac{n\pi v}{L}\right)t] \\
& +\sum_{n=1}^{\infty}e^{-\xi_n\omega_n t}\times\Bigg[-\frac{m_{v,1}gL^3}{n^4\pi^4 EI}\times\frac{2\xi_n(n\pi v/L\omega_n)}{[1-(n\pi v/L\omega_n)^2]^2+[2\xi_n(n\pi v/L\omega_n)]^2}-\frac{m_{v,2}gL^3}{n^4\pi^4 EI}\times\cos\frac{n\pi vt_s}{L}\times\frac{2\xi_n(n\pi v/L\omega_n)}{[1-(n\pi v/L\omega_n)^2]^2+[2\xi_n(n\pi v/L\omega_n)]^2} \\
& -\frac{m_{v,2}gL^3}{n^4\pi^4 EI}\times\sin\frac{n\pi vt_s}{L}\times\frac{((n\pi v/L\omega_n)^2-1)}{[1-(n\pi v/L\omega_n)^2]^2+[2\xi_n(n\pi v/L\omega_n)]^2}\Bigg]\times[\sin\left(\omega_n\sqrt{1-\xi_n^2}+\frac{n\pi v}{L}\right)t-\sin\left(\omega_n\sqrt{1-\xi_n^2}-\frac{n\pi v}{L}\right)t]
\end{aligned}
\tag{10}
$$

Substituting Equation (10) into Equation (1) also yields the displacement $u_{v1}(t)$ of the test vehicle.

Practically, the response component associated with the n^{th} modal frequency of the bridge can be separated from the response of the test vehicle [29] by a band-pass filter with limits

$\omega_n\sqrt{1-\xi_n^2}-n\pi v/L$ and $\omega_n\sqrt{1-\xi_n^2}+n\pi v/L$, due to the different coupling degree of vehicle and bridge considered in the theoretical solution, the filtering range will be adjusted appropriately in the following section of numerical simulation [15]. The resulting signal is the transient response from the n^{th} vibration mode of the bridge structure, which is directly related to the last term on the right-hand-side (RHS) of Equation (10).

Substituting the last term of Equation (10) into Equation (1), the vehicle displacement $u_{v1}(t)$ related to the n^{th} mode shape of the deck is obtained as:

$$\begin{aligned}u_{v1}(t)=&\sum_{n=1}^{\infty}e^{-\xi_n\omega_n t}\times\frac{\xi_{v1}A_n}{2\sqrt{1-\xi_{v1}^2}}\times[\frac{(\omega_n\sqrt{1-\xi_n^2}+n\pi v/L)(\xi_n\omega_n-\xi_{v1}\omega_{v1})-\xi_n\omega_n(\omega_n\sqrt{1-\xi_n^2}+n\pi v/L+\omega_{v1}\sqrt{1-\xi_{v1}^2})}{(\xi_n\omega_n-\xi_{v1}\omega_{v1})^2+(\omega_n\sqrt{1-\xi_n^2}+n\pi v/L+\omega_{v1}\sqrt{1-\xi_{v1}^2})^2}\\&-\frac{(\omega_n\sqrt{1-\xi_n^2}+n\pi v/L)(\xi_n\omega_n-\xi_{v1}\omega_{v1})-\xi_n\omega_n(\omega_n\sqrt{1-\xi_n^2}+n\pi v/L-\omega_{v1}\sqrt{1-\xi_{v1}^2})}{(\xi_n\omega_n-\xi_{v1}\omega_{v1})^2+(\omega_n\sqrt{1-\xi_n^2}+n\pi v/L-\omega_{v1}\sqrt{1-\xi_{v1}^2})^2}]\times\sin(\omega_n\sqrt{1-\xi_n^2}+\frac{n\pi v}{L})t\\&+\sum_{n=1}^{\infty}e^{-\xi_n\omega_n t}\times\frac{\xi_{v1}A_n}{2\sqrt{1-\xi_{v1}^2}}\times[\frac{(\omega_n\sqrt{1-\xi_n^2}-n\pi v/L)(\xi_n\omega_n-\xi_{v1}\omega_{v1})+\xi_n\omega_n(\omega_n\sqrt{1-\xi_n^2}-n\pi v/L+\omega_{v1}\sqrt{1-\xi_{v1}^2})}{(\xi_n\omega_n-\xi_{v1}\omega_{v1})^2+(\omega_n\sqrt{1-\xi_n^2}-n\pi v/L+\omega_{v1}\sqrt{1-\xi_{v1}^2})^2}\\&-\frac{(\omega_n\sqrt{1-\xi_n^2}-n\pi v/L)(\xi_n\omega_n-\xi_{v1}\omega_{v1})+\xi_n\omega_n(\omega_n\sqrt{1-\xi_n^2}-n\pi v/L-\omega_{v1}\sqrt{1-\xi_{v1}^2})}{(\xi_n\omega_n-\xi_{v1}\omega_{v1})^2+(\omega_n\sqrt{1-\xi_n^2}-n\pi v/L-\omega_{v1}\sqrt{1-\xi_{v1}^2})^2}]\times\sin(\omega_n\sqrt{1-\xi_n^2}-\frac{n\pi v}{L})t\\=&\sum_{n=1}^{\infty}P_n e^{-\xi_n\omega_n t}-\sum_{n=1}^{\infty}R_n e^{-\xi_n\omega_n t}\end{aligned}\tag{11}$$

where the vehicle damping ratio is $\xi_{v1}=c_{v1}/(2m_{v1}\omega_{v1})$ and

$$\begin{aligned}A_n=&-\frac{2m_{v,1}gL^3}{n^4\pi^4EI}\times\frac{2\xi_n(n\pi v/L\omega_n)}{[1-(n\pi v/L\omega_n)^2]^2+[2\xi_n(n\pi v/L\omega_n)]^2}-\frac{2m_{v,2}gL^3}{n^4\pi^4EI}\times\cos\frac{n\pi vt_s}{L}\times\frac{2\xi_n(n\pi v/L\omega_n)}{[1-(n\pi v/L\omega_n)^2]^2+[2\xi_n(n\pi v/L\omega_n)]^2}\\&-\frac{2m_{v,2}gL^3}{n^4\pi^4EI}\times\sin\frac{n\pi vt_s}{L}\times\frac{((n\pi v/L\omega_n)^2-1)}{[1-(n\pi v/L\omega_n)^2]^2+[2\xi_n(n\pi v/L\omega_n)]^2}\end{aligned}\tag{12}$$

Only a single vibration mode of the deck is needed for damage identification [1,45,47] in the improved DSC method. Because of the difficulty and accuracy of acquiring higher mode on site cannot be guaranteed, the terms frequency and mode shape in the following discussions are referred to those of the first vibration mode of the deck unless otherwise stated. The response component R_1 of the test vehicle associated with the 1st vibration mode of the bridge deck can also be written as:

$$R_1=e^{-\xi_1\omega_1 t}\left\{A_1\sin\left[\left(\omega_1\sqrt{1-\xi_1^{\,2}}+\frac{\pi v}{L}\right)t\right]+A_2\sin\left[\left(\omega_1\sqrt{1-\xi_1^{\,2}}-\frac{\pi v}{L}\right)t\right]\right\}\tag{13}$$

The coefficients A_1 to A_2 can be determined by comparing terms in Equations (9) and (10) as:

$$\begin{aligned}A_1=&\frac{\xi_{v1}A}{2\sqrt{1-\xi_{v1}^2}}\times[\frac{(\omega_1\sqrt{1-\xi_1^2}+n\pi v/L)(\xi_1\omega_1-\xi_{v1}\omega_{v1})-\xi_1\omega_1(\omega_1\sqrt{1-\xi_1^2}+\pi v/L+\omega_{v1}\sqrt{1-\xi_{v1}^2})}{(\xi_1\omega_1-\xi_{v1}\omega_{v1})^2+(\omega_1\sqrt{1-\xi_1^2}+\pi v/L+\omega_{v1}\sqrt{1-\xi_{v1}^2})^2}\\&-\frac{(\omega_1\sqrt{1-\xi_1^2}+n\pi v/L)(\xi_1\omega_1-\xi_{v1}\omega_{v1})-\xi_1\omega_1(\omega_1\sqrt{1-\xi_1^2}+\pi v/L-\omega_{v1}\sqrt{1-\xi_{v1}^2})}{(\xi_1\omega_1-\xi_{v1}\omega_{v1})^2+(\omega_1\sqrt{1-\xi_1^2}+\pi v/L-\omega_{v1}\sqrt{1-\xi_{v1}^2})^2}]\end{aligned}\tag{14}$$

$$\begin{aligned}A_2=&\frac{\xi_{v1}A}{2\sqrt{1-\xi_{v1}^2}}\times[\frac{(\omega_1\sqrt{1-\xi_1^2}-\pi v/L)(\xi_1\omega_1-\xi_{v1}\omega_{v1})+\xi_1\omega_1(\omega_1\sqrt{1-\xi_1^2}-\pi v/L+\omega_{v1}\sqrt{1-\xi_{v1}^2})}{(\xi_1\omega_1-\xi_{v1}\omega_{v1})^2+(\omega_1\sqrt{1-\xi_1^2}-\pi v/L+\omega_{v1}\sqrt{1-\xi_{v1}^2})^2}\\&-\frac{(\omega_1\sqrt{1-\xi_1^2}-\pi v/L)(\xi_1\omega_1-\xi_{v1}\omega_{v1})+\xi_1\omega_1(\omega_1\sqrt{1-\xi_1^2}-\pi v/L-\omega_{v1}\sqrt{1-\xi_{v1}^2})}{(\xi_1\omega_1-\xi_{v1}\omega_{v1})^2+(\omega_1\sqrt{1-\xi_1^2}-\pi v/L-\omega_{v1}\sqrt{1-\xi_{v1}^2})^2}]\end{aligned}\tag{15}$$

The corresponding acceleration response component of the first vibration mode of the deck can also be obtained as:

$$\ddot{R}_1 = e^{-\xi_1\omega_1 t}\left\{\bar{\bar{A}}_1 \sin\left[\left(\omega_1\sqrt{1-\xi_1^2}+\frac{\pi v}{L}\right)t\right]+\bar{\bar{A}}_2 \sin\left[\left(\omega_1\sqrt{1-\xi_1^2}-\frac{\pi v}{L}\right)t\right]\right\} \tag{16}$$

where the coefficients $\bar{\bar{A}}_1$ to $\bar{\bar{A}}_2$ are:

$$\bar{\bar{A}}_1 = \left[\left(\omega_1\sqrt{1-\xi_1^2}+\pi v/L\right)+\xi_1^2\omega_1^2\right]\times A_1, \qquad \bar{\bar{A}}_2 = -\left[\left(\omega_1\sqrt{1-\xi_1^2}-\pi v/L\right)+\xi_1^2\omega_1^2\right]\times A_2 \tag{17}$$

If the transient effect is ignored, $\ddot{R}_1/e^{-\xi_1\omega_1 t}$ can be introduced as:

$$\ddot{R}_{11} = \ddot{R}_1/e^{-\xi_1\omega_1 t} = \bar{\bar{A}}_1 \sin\left[\left(\omega_1\sqrt{1-\xi_1^2}+\frac{\pi v}{L}\right)t\right]+\bar{\bar{A}}_2 \sin\left[\left(\omega_1\sqrt{1-\xi_1^2}-\frac{\pi v}{L}\right)t\right] \tag{18}$$

It should be noted that Equation (16) is similar to Equation (22) of Reference [9] and Equation (23) of Reference [28] but with the inclusion of the vehicle and bridge damping. It is also noted that all the variables of the test vehicle, tractor, and bridge in Equations (14) and (15) are constant. This implies that the coefficients $\bar{\bar{A}}_1$ to $\bar{\bar{A}}_2$ are constant for constant vehicle speed. The bridge response component $\ddot{R}_{11}$ in Equation (18) can be Hilbert transformed to yield.

$$H\left[\ddot{R}_{11}\right] = \bar{\bar{A}}_1 \cos\left[\left(\omega_1\sqrt{1-\xi_1^2}+\frac{\pi v}{L}\right)t\right]+\bar{\bar{A}}_2 \cos\left[\left(\omega_1\sqrt{1-\xi_1^2}-\frac{\pi v}{L}\right)t\right] \tag{19}$$

For the case when $\pi v/L$ of the test vehicle is negligibly small compared with the 1st modal frequency of the bridge $\omega_1\sqrt{1-\xi_1^2}$, i.e., $\pi v/L \ll \omega_1\sqrt{1-\xi_1^2}$, the instantaneous amplitude can be obtained as:

$$A(t) = \sqrt{\ddot{R}_{11}^2 + H\left[\ddot{R}_{11}\right]^2} = \sqrt{\left(\bar{\bar{A}}_1+\bar{\bar{A}}_2\right)^2 - 4\bar{\bar{A}}_1\bar{\bar{A}}_2\sin^2\left(\frac{\pi v t}{L}\right)} = 2\sqrt{\bar{\bar{A}}_1\bar{\bar{A}}_2}\left|\sin\frac{\pi v t}{L}\right| \tag{20}$$

Replacing x by vt in Equation (20) yields:

$$A\left(\frac{x}{v}\right) = 2\sqrt{\bar{\bar{A}}_1\bar{\bar{A}}_2}\left|\sin\frac{\pi x}{L}\right| \tag{21}$$

Equation (21) shows that the instantaneous amplitude $A(x/v)$ of the estimated acceleration response component is the 1st vibration mode shape component of the bridge deck (in the absolute sense) multiplied by a scalarof $2\sqrt{\bar{\bar{A}}_1\bar{\bar{A}}_2}$. Therefore, once the acceleration response component is obtained from the measured response of the test vehicle as shown in Equation (18), it can be normalized with $e^{-\xi_1\omega_1 t}$ to remove the transient effect of the response followed by Hilbert transformation to get the scale factor [9] of the first vibration mode shape of the bridge deck. It is worth noting that although the theoretical part of this paper uses the simple supported beam bridge mode under the undamaged condition, the numerical simulation analysis based on the damaged conditions below shows that the technique is also suitable for damage identification.

2.2. Element Bending Stiffness of Beam from the Improved DSC Method

The improved DSC method used the moment-curvature relationship for calculating the bending stiffness EI of the beam [1,45,47] as:

$$EI = \frac{M}{d^2\varphi/dx^2} = \frac{M}{\kappa} \tag{22}$$

where φ is the mode shape and κ the modal curvature of the beam. This equation is valid for the case with a Euler-Bernoulli beam. Considering a beam segment from x_i to x_{i+1} in Figure 2a, the bending moment M_{i+1} at x_{i+1} is computed based on D'Alembert's principle from the equilibrium condition of the segment including the inertial force as [1,45,47]:

$$M_{i+1} = M_i - \int_{x_i}^{x_{i+1}} \omega_1^2 \rho A \varphi(x)(x_{i+1} - x)dx + V_i(x_{i+1} - x_i) \tag{23}$$

And

$$V_{i+1} = V_i - \int_{x_i}^{x_{i+1}} \omega_1^2 \rho A \varphi(x)dx \tag{24}$$

where V_i and M_i are the shear force and bending moment at x_i respectively, ω_1 and ϕ are the 1st modal frequency and mode shape of the beam, respectively, ρ is the material density, and *A*isthe cross-sectional area of the beam. The end forces V_0 and M_0 are depending on the inertia force of the entire beam.

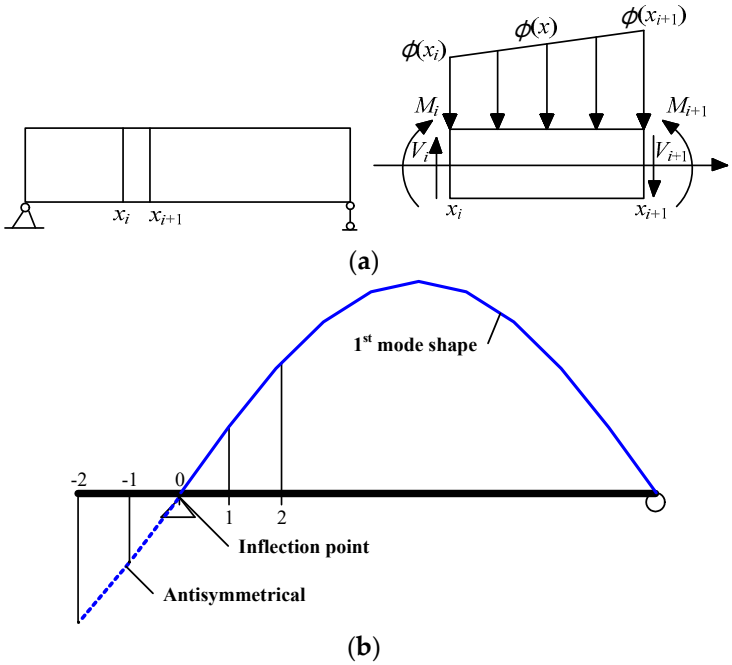

Figure 2. Member forces and modal displacements: (**a**) Sign convention of internal forces; (**b**) 1st mode shape extrapolation.

Curvature κ of the mode shape is calculated by the central difference method [1,45,47]. The numerical problem of zero mode shape value at the simply-supported ends of the beam is improved in this study by extrapolating the mode shape taking the ends of the beam as inflection points as shown in Figure 2b. The bending stiffness *EI* of the beam calculated from Equation (22) is then used for damage identification.

2.3. Reducing the Effect of Road Surface Roughness

The equations of motion in Equations (1)–(3) can be modified to include the road surface roughness $r(x)$ as:

$$m_{v1}\ddot{u}_{v1}(t) + k_{v1}(u_{v1}(t) - u(x,t)\big|_{x=vt} - r(x)\big|_{x=vt}) + c_{v1}(\dot{u}_{v1}(t) - \dot{u}(x,t)\big|_{x=vt} - \dot{r}(x)\big|_{x=vt}) = 0 \tag{25}$$

$$m_{v2}\ddot{u}_{v2}(t) + k_{v2}(u_{v2}(t) - u(x,t)\big|_{x=vt_a} - r(x)\big|_{x=vt_a}) + c_{v2}(\dot{u}_{v2}(t) - \dot{u}(x,t)\big|_{x=vt_a} - \dot{r}(x)\big|_{x=vt_a}) = 0 \tag{26}$$

$$m^*\ddot{u}(x,t) + c\dot{u}(x,t) + EIu''''(x,t) = f_{c1}(t)\delta(x - vt) + f_{c2}(t)\delta(x - vt_a) \tag{27}$$

where the interaction force $f_{c1}(t)$, $f_{c2}(t)$ becomes respectively:

$$f_{c1}(t)=-m_{v1}g+k_{v1}\left[u_{v1}(t)-u(x,t)\Big|_{x=vt}-r(x)\Big|_{x=vt}\right]+c_{v1}\left[\dot{u}_{v1}(t)-\dot{u}(x,t)\Big|_{x=vt}-\dot{r}(x)\Big|_{x=vt}\right] \tag{28}$$

$$f_{c2}(t)=-m_{v2}g+k_{v2}\left[u_{v2}(t)-u(x,t)\Big|_{x=vt_a}-r(x)\Big|_{x=vt_a}\right]+c_{v2}\left[\dot{u}_{v2}(t)-\dot{u}(x,t)\Big|_{x=vt_a}-\dot{r}(x)\Big|_{x=vt_a}\right] \tag{29}$$

Accordingly, the n^{th} modal equation of the deck in Equation (7) can be modified as:

$$\begin{aligned}\ddot{q}_n(t)+2\xi_n\omega_n\dot{q}_n(t)+\omega_n^2q_n(t)=2\sin\frac{n\pi vt}{L}\{&-\frac{m_{v1}g}{m^*L}-\frac{m_{v2}g}{m^*L}+\frac{m_{v1}\omega_{v1}^2}{m^*L}\left[u_{v1}(t)-u(x,t)\Big|_{x=vt}-r(x)\Big|_{x=vt}\right]\\&+\frac{2m_{v1}\omega_{v1}\xi_{v1}}{m^*L}(\dot{u}_{v1}(t)-\dot{u}(x,t)\Big|_{x=vt}-\dot{r}(x)\Big|_{x=vt})+\frac{m_{v2}\omega_{v2}^2}{m^*L}\left[u_{v2}(t)-u(x,t)\Big|_{x=vt_a}-r(x)\Big|_{x=vt_a}\right]\\&+\frac{2m_{v2}\omega_{v2}\xi_{v2}}{m^*L}(\dot{u}_{v2}(t)-\dot{u}(x,t)\Big|_{x=vt_a}-\dot{r}(x)\Big|_{x=vt_a})\}\end{aligned} \tag{30}$$

It is noted that the last four terms on the RHS of Equation (30) are much less than the two terms. Equation (30) will be reduced to Equation (7) if they are ignored. This is consistent with the observation by Yau et al. [48,49] that the dynamic effect of a moving vehicle caused by the road profile has a negligible influence on the bridge response even in the road surface roughness of Class D as given in ISO 8608 [50]. It is noted that this simplification is for the briefness of derivations in this section and subsequent discussions do not affect the purpose of the demonstration. To be more realistic, this ignoring effect is all included in the finite element modeling and numerical analysis later.

Meanwhile, the effect of road surface roughness on the vehicle response should not be ignored, and Equation (25) can be rewritten as:

$$\ddot{u}_{v1}(t)+2\xi_{v1}\omega_{v1}\dot{u}_{v1}(t)+\omega_{v1}^2u_{v1}(t)=\omega_{v1}^2(r(x)\Big|_{x=vt}+u(x,t)\Big|_{x=vt})+2\omega_{v1}\xi_{v1}(\dot{r}(x)\Big|_{x=vt}+\dot{u}(x,t)\Big|_{x=vt}) \tag{31}$$

According to Duhamel integration,

$$\ddot{u}_{v1,r}(t)=\frac{1}{\sqrt{1-\xi_{v1}^2}}\int_0^t\left\{\omega_{v1}[r(x)\Big|_{x=vt}]+2\xi_{v1}[\dot{r}(x)\Big|_{x=vt}]\right\}e^{-\xi_{v1}\omega_{v1}(t-\tau)}[\sin\omega_{v1}\sqrt{1-\xi_{v1}^2}(t-\tau)]d\tau \tag{32}$$

In Equation (32), the effect of road surface roughness on the test vehicle response is an independent term only variation with parameters of vehicle frequency ω_{v1}, damping ratio ξ_{v1}. It indicates that the residual response, i.e., the response of the No.1 test vehicle subtracted by that of the No.2 test vehicle towed under the same tractor respectively, could be a good choice to remove the road surface roughness effect.

The paper [21] makes use of two identical test vehicles going across the bridge at one time for removing the effect of road surface roughness in the identification of bridge modal frequencies and mode shape without considering the bridge and vehicle damping ratio and coupling effects between the test vehicle and bridge. It is based on one case of two test vehicles going across the bridge with a spacing distance at one time but the theory is deduced from the single vehicle-bridge couple system [21], this is a contradiction between theoretical derivation and numerical simulation.

The present study proposes a general configuration of two test vehicles with identical modal frequency and damping ratio, but with the mass, stiffness, and damping coefficients of the No.2 test vehicle proportional to those of the No.1 test vehicle, as shown in Figure 1, moving across the bridge alone respectively towed under the same tractor. i.e., this is two cases of the single vehicle with the same tractor going across the bridge respectively. According to Equation (11), the difference between the responses of the two test vehicles, i.e., $\Delta u(t)=u_{v,No.2}(t)-u_{v,No.1}(t)$, related to the n^{th} mode shape of the deck can be expressed as:

$$\begin{aligned}\Delta u(t)=&\sum_{n=1}^{\infty}e^{-\xi_n\omega_n t}\times\frac{\xi_{v1}\Delta A}{2\sqrt{1-\xi_{v1}^2}}\times[\frac{(\omega_n\sqrt{1-\xi_n^2}+n\pi v/L)(\xi_n\omega_n-\xi_{v1}\omega_{v1})-\xi_n\omega_n(\omega_n\sqrt{1-\xi_n^2}+n\pi v/L+\omega_{v1}\sqrt{1-\xi_{v1}^2})}{(\xi_n\omega_n-\xi_{v1}\omega_{v1})^2+(\omega_n\sqrt{1-\xi_n^2}+n\pi v/L+\omega_{v1}\sqrt{1-\xi_{v1}^2})^2}\\&-\frac{(\omega_n\sqrt{1-\xi_n^2}+n\pi v/L)(\xi_n\omega_n-\xi_{v1}\omega_{v1})-\xi_n\omega_n(\omega_n\sqrt{1-\xi_n^2}+n\pi v/L-\omega_{v1}\sqrt{1-\xi_{v1}^2})}{(\xi_n\omega_n-\xi_{v1}\omega_{v1})^2+(\omega_n\sqrt{1-\xi_n^2}+n\pi v/L-\omega_{v1}\sqrt{1-\xi_{v1}^2})^2}]\times\sin(\omega_n\sqrt{1-\xi_n^2}+\frac{n\pi v}{L})t\\&+\sum_{n=1}^{\infty}e^{-\xi_n\omega_n t}\times\frac{\xi_{v1}\Delta A}{2\sqrt{1-\xi_{v1}^2}}\times[\frac{(\omega_n\sqrt{1-\xi_n^2}-n\pi v/L)(\xi_n\omega_n-\xi_{v1}\omega_{v1})+\xi_n\omega_n(\omega_n\sqrt{1-\xi_n^2}-n\pi v/L+\omega_{v1}\sqrt{1-\xi_{v1}^2})}{(\xi_n\omega_n-\xi_{v1}\omega_{v1})^2+(\omega_n\sqrt{1-\xi_n^2}-n\pi v/L+\omega_{v1}\sqrt{1-\xi_{v1}^2})^2}\\&-\frac{(\omega_n\sqrt{1-\xi_n^2}-n\pi v/L)(\xi_n\omega_n-\xi_{v1}\omega_{v1})+\xi_n\omega_n(\omega_n\sqrt{1-\xi_n^2}-n\pi v/L-\omega_{v1}\sqrt{1-\xi_{v1}^2})}{(\xi_n\omega_n-\xi_{v1}\omega_{v1})^2+(\omega_n\sqrt{1-\xi_n^2}-n\pi v/L-\omega_{v1}\sqrt{1-\xi_{v1}^2})^2}]\times\sin(\omega_n\sqrt{1-\xi_n^2}-\frac{n\pi v}{L})t\\=&\sum_{n=1}^{\infty}\Delta P_n e^{-\xi_n\omega_n t}-\sum_{n=1}^{\infty}\Delta R_n e^{-\xi_n\omega_n t}\end{aligned}\tag{33}$$

If the ratio of the mass, stiffness, and damping coefficients of the No.1 and No.2 test vehicles is 1:2, where ΔA is denoted as:

$$\Delta A=-\frac{2m_{v,1}gL^3}{n^4\pi^4EI}\times\frac{2\xi_n(n\pi v/L\omega_n)}{[1-(n\pi v/L\omega_n)^2]^2+[2\xi_n(n\pi v/L\omega_n)]^2}\tag{34}$$

Similar to Equation (11), the response component *R1* in Equation (13) can also be obtained from Equation (33). Because of no parameters of the tractor appearing in Equations (33) and (34), the effect of the tractor will be eliminated by the difference between the responses of the two test vehicles. It shows that no direct influence on the difference between the responses of the two test vehicles for the selected type of tractor.

For a single vehicle-bridge couple system without considering the tractor, the vehicle displacement response related to the n^{th} mode shape of the deck can also be deduced as:

$$\begin{aligned}u_{v1}(t)=&\sum_{n=1}^{\infty}e^{-\xi_n\omega_n t}\times\frac{\xi_{v1}}{\sqrt{1-\xi_{v1}^2}}\times\frac{-m_{v1}gL^3}{n^4\pi^4EI}\times\frac{2\xi_n(n\pi v/L\omega_n)}{[1-(n\pi v/L\omega_n)^2]^2+[2\xi_n(n\pi v/L\omega_n)]^2}\times[\frac{(\omega_n\sqrt{1-\xi_n^2}+n\pi v/L)(\xi_n\omega_n-\xi_{v1}\omega_{v1})-\xi_n\omega_n(\omega_n\sqrt{1-\xi_n^2}+n\pi v/L+\omega_{v1}\sqrt{1-\xi_{v1}^2})}{(\xi_n\omega_n-\xi_{v1}\omega_{v1})^2+(\omega_n\sqrt{1-\xi_n^2}+n\pi v/L+\omega_{v1}\sqrt{1-\xi_{v1}^2})^2}\\&-\frac{(\omega_n\sqrt{1-\xi_n^2}+n\pi v/L)(\xi_n\omega_n-\xi_{v1}\omega_{v1})-\xi_n\omega_n(\omega_n\sqrt{1-\xi_n^2}+n\pi v/L-\omega_{v1}\sqrt{1-\xi_{v1}^2})}{(\xi_n\omega_n-\xi_{v1}\omega_{v1})^2+(\omega_n\sqrt{1-\xi_n^2}+n\pi v/L-\omega_{v1}\sqrt{1-\xi_{v1}^2})^2}]\times\sin(\omega_n\sqrt{1-\xi_n^2}+n\pi v/L)t\\&+\sum_{n=1}^{\infty}e^{-\xi_n\omega_n t}\times\frac{\xi_{v2}}{\sqrt{1-\xi_{v2}^2}}\times\frac{-m_{v1}gL^3}{n^4\pi^4EI}\times\frac{2\xi_n(n\pi v/L\omega_n)}{[1-(n\pi v/L\omega_n)^2]^2+[2\xi_n(n\pi v/L\omega_n)]^2}\times[\frac{(\omega_n\sqrt{1-\xi_n^2}-n\pi v/L)(\xi_n\omega_n-\xi_{v2}\omega_{v2})-\xi_n\omega_n(\omega_n\sqrt{1-\xi_n^2}-n\pi v/L+\omega_{v2}\sqrt{1-\xi_{v2}^2})}{(\xi_n\omega_n-\xi_{v2}\omega_{v2})^2+(\omega_n\sqrt{1-\xi_n^2}-n\pi v/L+\omega_{v2}\sqrt{1-\xi_{v2}^2})^2}\\&-\frac{(\omega_n\sqrt{1-\xi_n^2}-n\pi v/L)(\xi_n\omega_n-\xi_{v1}\omega_{v1})-\xi_n\omega_n(\omega_n\sqrt{1-\xi_n^2}-n\pi v/L-\omega_{v1}\sqrt{1-\xi_{v1}^2})}{(\xi_n\omega_n-\xi_{v1}\omega_{v1})^2+(\omega_n\sqrt{1-\xi_n^2}-n\pi v/L-\omega_{v1}\sqrt{1-\xi_{v1}^2})^2}]\times\sin(\omega_n\sqrt{1-\xi_n^2}-n\pi v/L)t\\=&\left[\sum_{n=1}^{\infty}P_{n1}-\sum_{n=1}^{\infty}R_{n1}\right]e^{-\xi_n\omega_n t}\end{aligned}\tag{35}$$

Equations (33) and (35) show identical coefficients in the corresponding time function. For the determined vehicles and bridge parameters shown in Figure 1, $\Delta u(t)$ in Equation (33) will be equal to u_{v1} in Equation (35). It indicates that the difference between the responses of the two test vehicles will give the response from an equivalent vehicle of the single vehicle-bridge couple system with a smooth deck. It also can be noted that the residual acceleration of the two test vehicles $\Delta\ddot{u}(t)$ can be obtained by taking the second derivative of the residual displacement $\Delta u(t)$.

2.4. Effect of Ambient Temperature

Ambient temperature is the most influential factor amongst the different environmental effects affecting the dynamic properties of a structure. The removal of this effect is obligatory in the damage diagnosis of structures with vibration-based health monitoring [51,52].

One solution is to make reference to the correlation between the measured natural frequencies and the corresponding ambient temperature[51]. When the reference temperature is taken as 20 °C, the natural frequencies obtained from an ambient temperature can be adjusted to that under the reference temperature according to [52]

$$\omega_{20^\circ C}=\omega_{T^\circ C}\times\sqrt{\frac{E_{20^\circ C}}{E_{T^\circ C}}}=\omega_{T^\circ C}\times\sqrt{\frac{27.685}{-0.1022\Delta T+27.685}} \tag{36}$$

For conventional concrete materials structure, where $\Delta T=T-20$ is the temperature difference between ambient temperature in practice and the reference temperature; $\omega_{T^\circ C}$ is the modal frequency of the structure when under ambient temperature; $\omega_{20^\circ C}$ is the modal frequency at the reference temperature, and the subscript denotes the temperature of the variable. *E* is Young's modulus of the material and the subscript denotes the temperature of the variable. The application of Equation (36) is based on the assumption of a uniform distribution of the temperature field in the structure.

2.5. Analysis Procedure of Tractor-Test Vehicle Technique for Non-Destructive Testing

The bridge under investigation is assumed to be regularly monitored by the tractor-testvehicle technique, and acceleration responses of the two test vehicles are recorded respectively during each inspection and then transmitted to the remote computer platform for analysis. The response from the current inspection is regarded as from the (possible) damaged state and that of the previous inspection as from the undamaged state. If no damage is detected in the current state after analysis with the proposed strategy, the response recorded in the current inspection will be regarded as from the undamaged state and it will be compared with the next response recorded which will be a new possible damaged state.

The analysis procedure of TTVT for non-destructive testing with the proposed strategy is as follows:

(1) Record the acceleration responses of the two test vehicles in the undamaged state.
(2) Identify the first modal frequency of the bridge structure from spectra of the residual displacement $\Delta u(t)$ and corresponding residual acceleration $\Delta\ddot{u}(t)$, which indicate a vehicle response without the effect ofroad surface roughness based on tractor-test vehicle technique, in both the undamaged and damaged states of the structure. If the ambient temperature is different from the reference temperature, adjust the identified frequencies in both states to that at the reference temperature with Equation (36).
(3) Normalize the acceleration response components $\ddot{R}_1$ in Equation(16) for the first vibration mode of the deck with $e^{-\xi_1\omega_1 t}$ to remove the transient effect. After the 1st bridge frequency ω_1 is made available, one can extract the acceleration response components $\ddot{R}_1$ and the damping ratio of the 1st vibration mode of the deckassociated with ω_1 from the corresponding residual accelerationby any feasible signal processing tools.
(4) Then, obtaining the instantaneous amplitude history of the bridge component response for the 1st vibration mode shape. Performing the Hilbert transform to the decomposed bridge component response $\ddot{R}_{11}$ in Equation (18) yields its transform pair $H[\ddot{R}_{11}]$ in Equation (19). Then, one can obtain the instantaneous amplitude history $A(t)$ of the bridge component response using Equations (20) and (21).
(5) Construct the first vibration mode shape from of the component response by Equation (21), the curve of the instantaneous amplitude function $A(t)$ is representative of the mode shape of the bridge in absolute value. The sign of the 1st mode shape can be decided according to engineers' judgment or experience [9].
(6) Calculate the modal curvature κ of the beam using the mode shape ϕ obtained above by the central difference method with due correction described in Section 3.
(7) Calculate the bending moment *M* of the beam with Equation (23) for each monitored cross-section of the deck.
(8) Calculate the bending stiffness *EI* of the beam using Equation (22) for each monitored cross-section of the deck.

Similar processes are also applied to bridges in a damaged state.Therefore, the corresponding flowchart is presented in Figure 3.

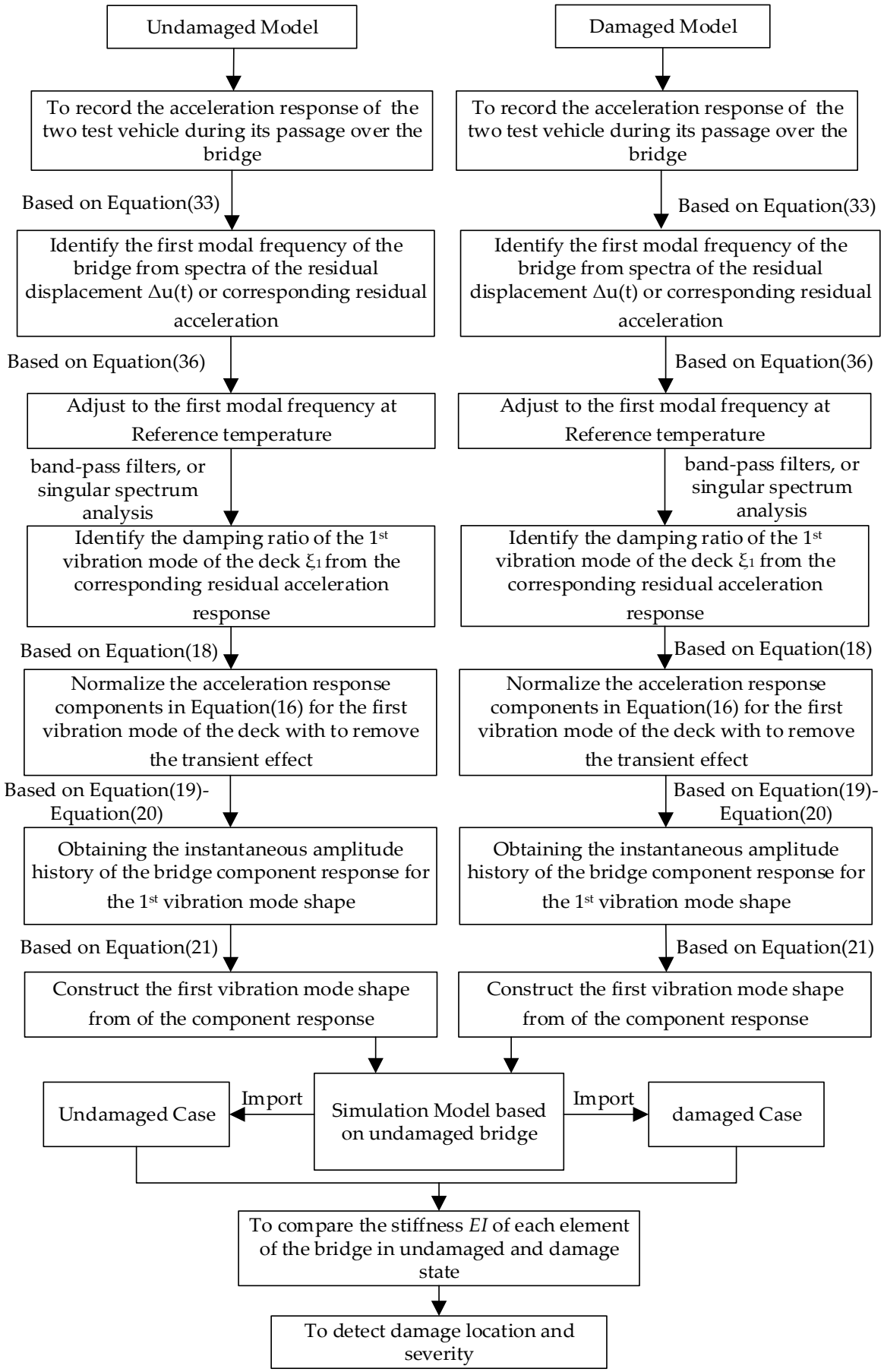

Figure 3. Flow chart of damage identification by using the tractor-test vehicle technique.

3. Numerical Study

The target bridge for the numerical study is the Da-Wu-Lun Bridge [5] located in northern Taiwan with 30 m simply-supported span and 16.5 m width deck. It composes of six prestressed I-girders at 2.8 m spacing with a 200 mm concrete deck slab and 50 mm asphaltic concrete surface layer as shown in Figure 4. The cross-sectional area and moment of inertia of each I-girder are 0.64 m^2 and 0.2422 m^4, respectively. The elastic modulus of concrete of the bridge is 29 GPa and the material density is 2400 kg/m^3. The 30 m span of the bridge is treated as a beam-like structure and it is discretized into 10 Euler-Bernoulli beamelements as shown in Figure 5. The element number is shown in circles and the numbers below the beam denote the node numbers. The time step of analysis is 0.01s, the *EI* value of the deck is calculated as $8.52\times10^{10} N\cdot m^2$ with the first modal frequency at 3.67 Hz and a damping ratio of 0.01. Class C [50] road surface roughness is considered. All these parameters are adopted in the following studies unless otherwise stated.

The assumptions of the TTVT of non-destructive testing are summarized for easy reference in the following studies: (1) The vehicle speed has to be constant to ensure a constant scale factor $2\sqrt{\bar{\bar{A}}_1\bar{\bar{A}}_2}$ in Equation (21); (2) The vehicle frequency $\pi v/L$ is negligibly small compared to the bridge modal parameters $\omega_1\sqrt{1-\xi_1^2}$ as required in the derivation of the instantaneous amplitude in Equation (19); and (3) The vehicle mass m_v is much less than those of the bridge in deriving Equation (7).

The following influential factors are studied: (a) the ratio of parameters in the two test vehicles; (b) vehicle speed v related to the first two limitations above; (c) modal frequency of vehicle ω_v related to the third limitation above;(d) the presence of road surface roughness; (e) the range value of bridge damping ratio; (f) the effect of measurement noise.

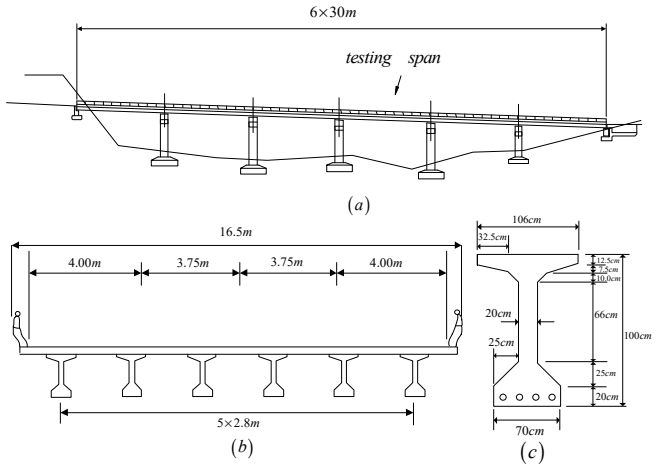

Figure 4. Bridge for simulation: (**a**) Elevation; (**b**) Cross-section; (**c**) Girder cross-section.

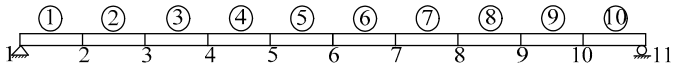

Figure 5. Discretization of the bridge into 10 beam elements.

3.1. Ratio of Vehicle Parameters

As for the vehicle-tractor-bridge couple system, any one of normal commercial vehicles chosen in China [53] can be regarded as a tractor, the parameters of the tractor in this simulation model are mass 10,000 kg, stiffness 2500 kN/m, and damping coefficient 30 $kN\cdot s/m$. The two test vehicles described in Table 1 are adopted, which requires special design and production. The No.1 and No.2 test vehicles go across the bridge deck respectively at a constant spacing of 2.0 m with the tractor. They will be applied to all cases below.

According to the technique presented above, letting both the No.1 test vehicle and No.2 test vehicle move over the bridge with the same roughness level respectively. Then, the response of the

No.1 test vehicle is subtracted from that of the No.2 test vehicle to obtain a response equivalent to the responses of the No.1 test vehicle moving over a smooth deck in a single vehicle-bridge system(withouta tractor). The difference between the responses of the two test vehicles with road surface roughness of Class C and the responses of the following No.1 test vehicle in a single vehicle-bridge system with a smooth road surface is shown in Figure 6. This example clearly demonstrated the applicability of the tractor-test vehicle technique for removing the road surface roughness effect in the construction of the mode shape of the bridge.

The study was repeated for the cases when the ratio of parameters of vehicles is 1:3, 1:4, and 1:5. The results are similar to that for the case with ratio 1:2 and, therefore, they are not shown.

Table 1. Properties of two test vehicles.

Properties of Test Vehicle	No.1	No.2
Frequency ω_v (Hz)	0.503	0.503
Mass m_v (kg)	5000	10,000
Stiffness k_v (kN/m)	50	100
Damping coefficient c_v kN · s/m	1	2
Speed v (m/s)	1	1

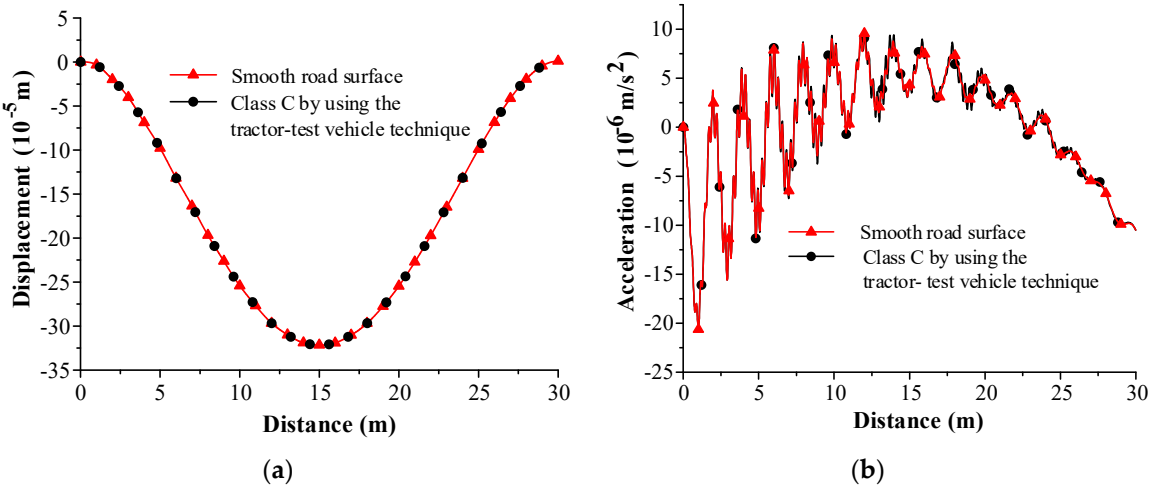

Figure 6. Comparison ofa single vehicle-bridge system (without tractor and roughness) and tractor-test vehicle technique (Class C road surface roughness): (**a**) Displacement; (**b**) Acceleration.

3.2. Effect of Constant Vehicle Speed

This section studies the range of constant vehicle speed that is applicable tothe estimation of the bridge mode shape and stiffness identification. All vehicles are allowed to go across the deck alone at three different constant speeds, i.e., 1, 2, and 3 m/s.

The bridge mode shape estimated from the difference between the responses of the two test vehicles is shown in Figure 7a. No obvious difference is found in the estimated mode shapes for the three vehicle speeds compared to the theoretical curve. The experimental fundamental frequency of the bridge deck in all three sets of results is 3.67 Hz, which is the same as the true value. The element bending stiffness *EI* of the bridge deck at the nodal points of the finite element model is computed with the improved DSC method described earlier and the results are shown in Figure 7b. The estimated *EI* from 1.0 m/s speed is clearly found closer to the true value with a maximum relative error less than 2%. This error becomes 16% and 20% for speeds at 2.0 and 3.0 m/s, respectively.

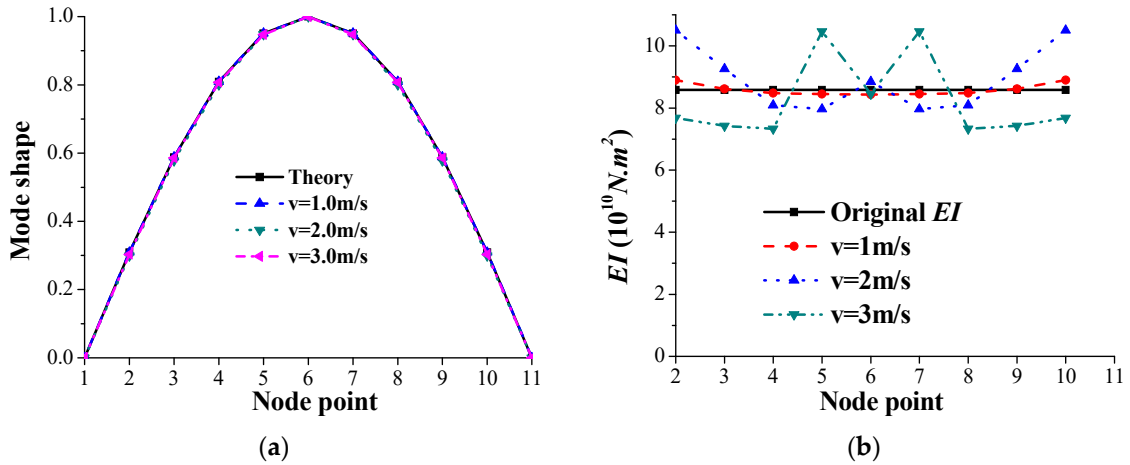

Figure 7. Identified resultsfor different vehicle speeds: (**a**) Mode shape and; (**b**) Element bending stiffness *EI*.

3.3. Effect of Non-Constant Vehicle Speed

The last part has studied that the effects of identified element bending stiffness on the bridge at a constant speed of 1 m/s is well matched with the theoretical results. Considering the field test, the running speed of the test vehicle (No.1 or No.2) and tractor are changed around 1m/s, and so the specific vehicle speed varies from 0.9875 m/s to 1.0125 m/s randomly in this section. The specific non-constant running speed of the test vehicle and tractor passing through the bridge is chosen as shown in Figure 8. According to the procedure of Figure 3, the 1st mode shape of the bridge and the identified element bending stiffness *EI* is shown in Figure 9. The maximum relative error between the theory value and identified results is also less than 2%. It indicated that when the running speed of the test vehicle changes within a certain range, it has little effect on the first-order modal and element bending stiffness values of the identified bridge.

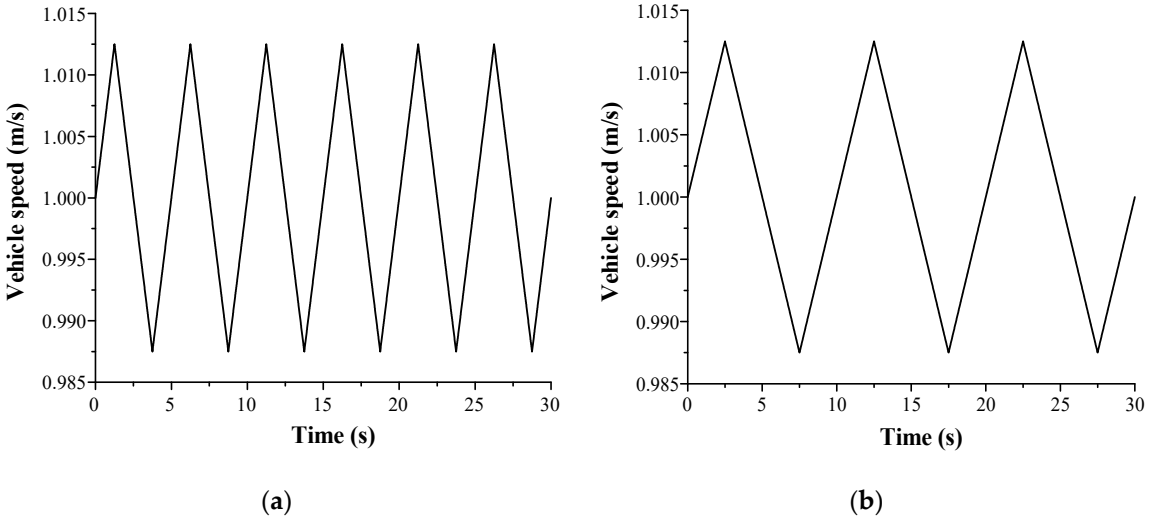

Figure 8. Non-constant running speed time history: (**a**) No.1 test vehicle;(**b**) No.2 test vehicle.

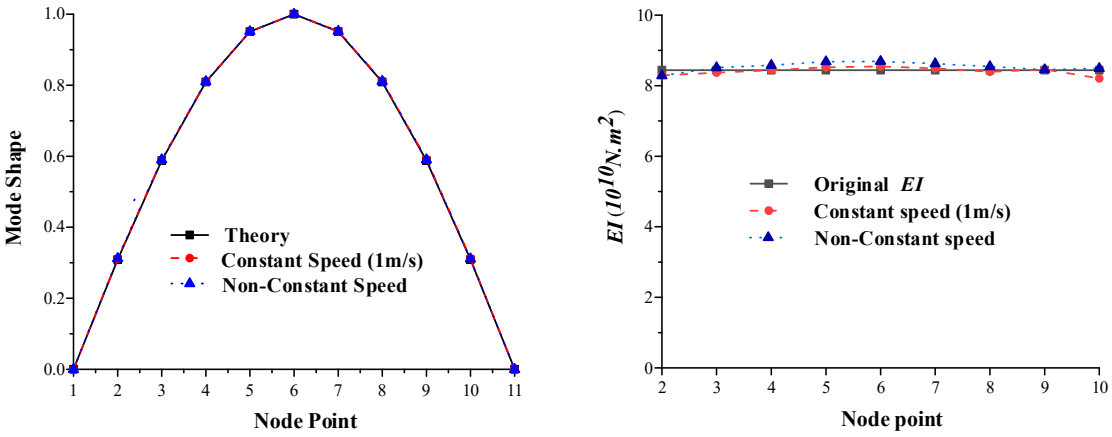

Figure 9. Identified results for non-constant speed: (**a**) Mode shape and; (**b**) Element bending stiffness *EI*.

3.4. Effect of Vehicle Modal Frequency

In this study, six No.1 test vehicles (No.1–1 to No.1–6) with different natural frequencies ω_v are shown in Table 2. The ratio of parameters of the No.1 and No.2 test vehicles is 1:2 but the frequency is the same. The bridge is assumed to have damping ratios of $\xi_n = 0.005, 0.01$ in the numerical study.

Table 2. Parameters of the six No.1 test vehicles.

Properties of the No.1 Test Vehicle	No.1-1	No.1-2	No.1-3	No.1-4	No.1-5	No.1-6
Frequency ω_v (Hz)	0.503	0.650	1.125	1.592	2.251	2.757
Mass m_v (Kg)	5000	3000	1000	500	1000	1000
Stiffness k_v (kN/m)	50	50	50	50	200	300
Damping coefficient c_v (kN · s/m)	1	1	1	1	1	1
Speed v (m/s)	1	1	1	1	1	1

The mode shape and estimated bending stiffness *EI* of the bridge deck obtained from the acceleration response of the two moving test vehicles are plotted in Figures 10 and 11. All the identified mode shapes from different vehicle frequencies and damping ratios are close to the theoretical one. The identified *EI* values at the bridge nodes differ slightly for different vehicle frequencies. The test vehicle with a lower frequency ω_v is noted to give more accurate estimation particularly close to the end of the beam. For the same test vehicle frequency, the relative error in the identified *EI* values is acceptable with a maximum less than 5% when the bridge damping ratio is less than 0.01. Further studies with higher damping ratios (not shown) show that the relative error becomes larger with higher bridge damping ratios. This may be due to the fact that a higher bridge damping ratio will lead to a larger phase difference in the structural responses at the locations of two vehicles causing a larger error in the difference of responses from the two vehicles. Specifically, the identified *EI* values are most accurate at the lowest vehicle modal frequency studied at $\omega_v = 0.503$ Hz.

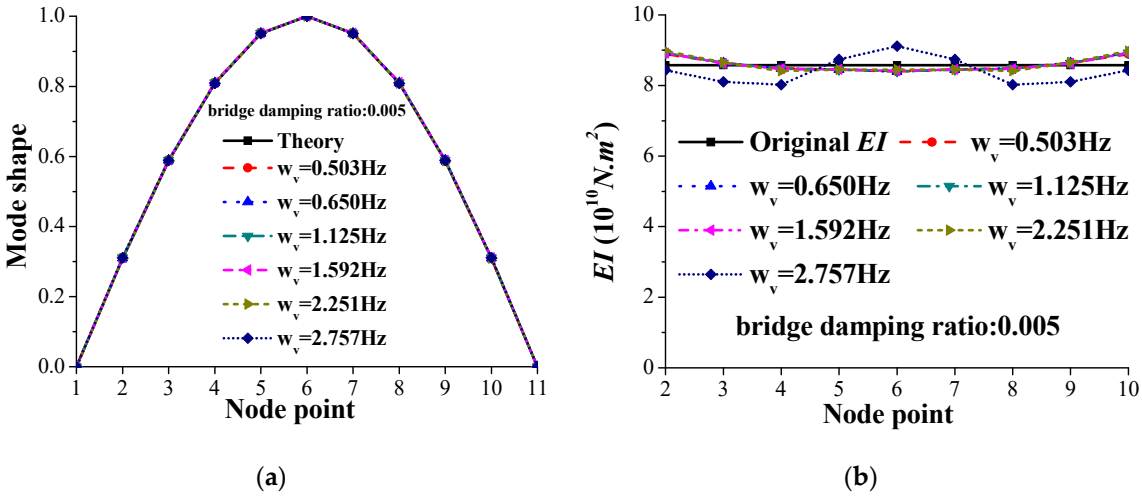

Figure 10. Identified results for different vehicle frequencies with bridge damping ratio ξ_n =0.005: (**a**) Mode shape; (**b**) Element bending stiffness *EI*.

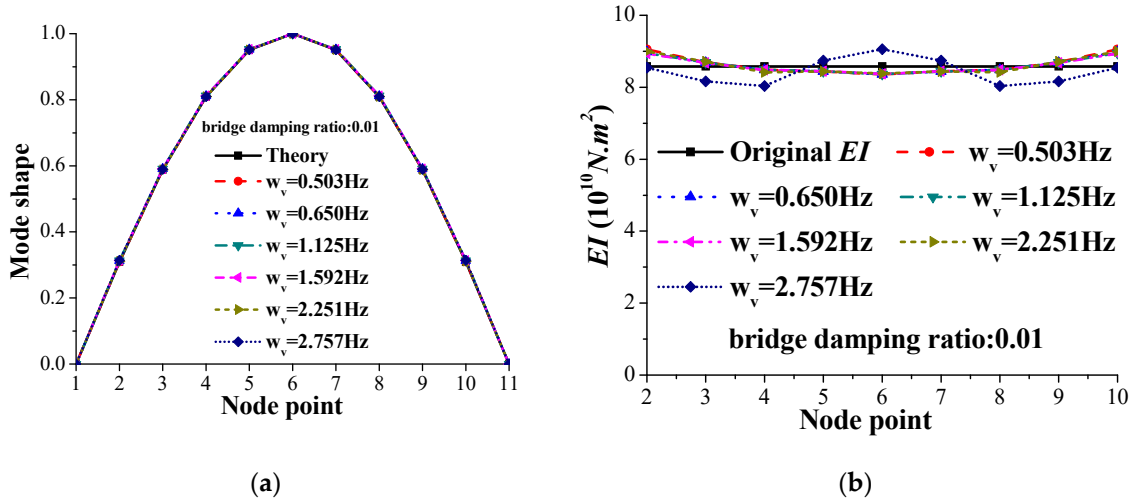

Figure 11. Identified results for different vehicle frequencies with bridge damping ratio ξ_n =0.01: (**a**) Mode shape; (**b**) Element bending stiffness *EI*.

3.5. Effect of Road Surface Roughness

The test vehicles described in Table 1, the tractor and bridge structure mentioned above are adopted in this study. The road surface roughness $r(x)$ generated by the power spectrum density (PSD) function can be expressed as follows:

$$r(x) = \sum_i d_i \cos(n_{s,i} x + \theta_i) \quad (37)$$

where $n_{s,i}$ is the i^{th} circle spatial frequency considered, θ_i the random phase angle of the i^{th} cosine function, and d_i the amplitude for each class of roughness selected, defined as $d_i = \sqrt{2G_d(n_i)\Delta n}$. Three classes of road surface roughness [50] are considered with the functional $G_d(n_0)$ in the PSD function of the road surface roughness defined as $G_d(n_i) = G_d(n_0)\left(\frac{n_i}{n_0}\right)^{-w}$, where n_i denotes the i^{th} spatial frequency per meter, w is a constant equal to 2, n_0 = 0.1 cycle/m. $G_d(n_0)$ is related to the class of roughness as given in ISO 8608 [50] and it equals to 16×10^{-6}㎥, 64×10^{-6}㎥ and 256×10^{-6}㎥

for Classes A, B, and C road surface roughness, respectively. It is noted that each case of adding road surface roughness is different even in the same Class level because of randomness.

The tractor-test vehicle technique was applied to get the mode shape of the bridge deck as shown in Figure 12a. No notable difference can be observed in the results for the three classes of roughness. The distribution of the identified element bending stiffness *EI* of the bridge in Figure 12b shows a better result for a smoother deck surface. The largest relative error in the identified element bending stiffness is less than 3% for all roughnessbut there is a large error at the end nodes 2 and 10, and the maximum error is less than 6% and 10%, respectively for class C roughness.

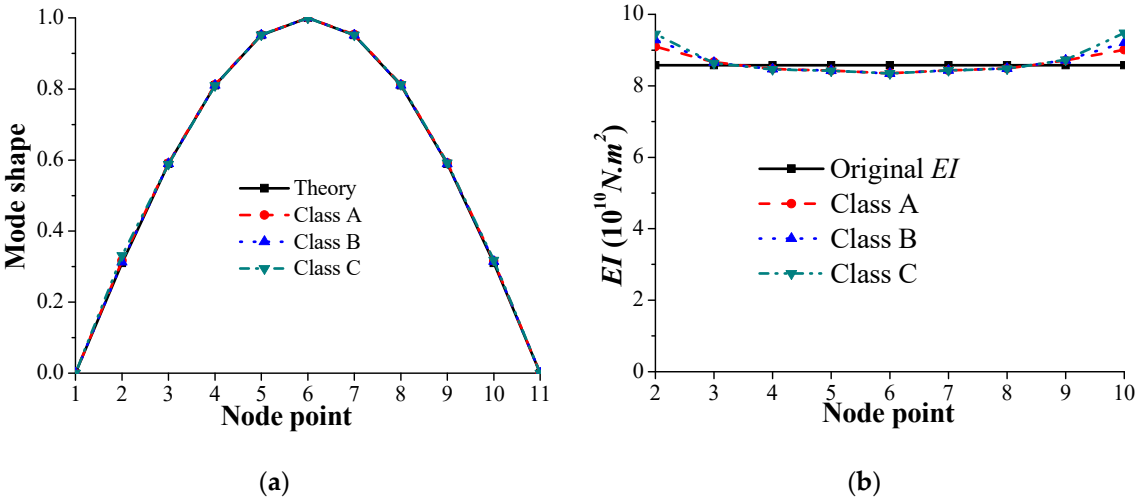

(**a**) (**b**)

Figure 12. Identified resultsfor three classes of road surface roughness with bridge damping ratio $\xi_n = 0.01$:(**a**) Mode shape; (**b**) Element bending stiffness *EI*.

3.6. Effect of Bridge Damping Ratio

Based on Equations (13)–(21) and step 3 of Section 2.5, the $e^{-\xi_1 \omega_1 t}$ is a time-variant quantity. The attenuation effect of the bridge's first-order frequency response is different under different bridge damping ratio conditions. A larger bridge damping ratio may cause it to decay in a short time, thereby adversely affecting the modal identification. Therefore, it is necessary to study the influence of the bridge damping ratio on the tractor-test vehicle technique.

The test vehicles in Table 1, the tractor and the bridge structure inthe last section are adopted, but the different bridge damping ratio ξ_n=0, 0.005, 0.01, 0.013, 0.015 is included in the bridge model, respectively. Additionally, the vehicle-tractor-bridge system studied in the last section is adopted with additional Class C road surface roughness on the bridge deck.

Figure 13 shows the results of the identified mode shape and undamaged *EI* with different bridge damping ratio. And the damage scenario with identified damaged *EI* for different damping ratios can be calculated for studying. Although there is no distinctive difference with the identified mode shape, all the results indicate that the identified *EI* is worse with a higher bridge damping ratio. Especially for the identified boundary element *EI* with higher bridge damping ratio ξ_n=0.013, 0.015, the errors compared with the original *EI* are more than 10%. It is suggested that the range value of bridge damping ratio is between 0 and 0.01 for preferable bridge damage identification based on the tractor-test vehicle technique.

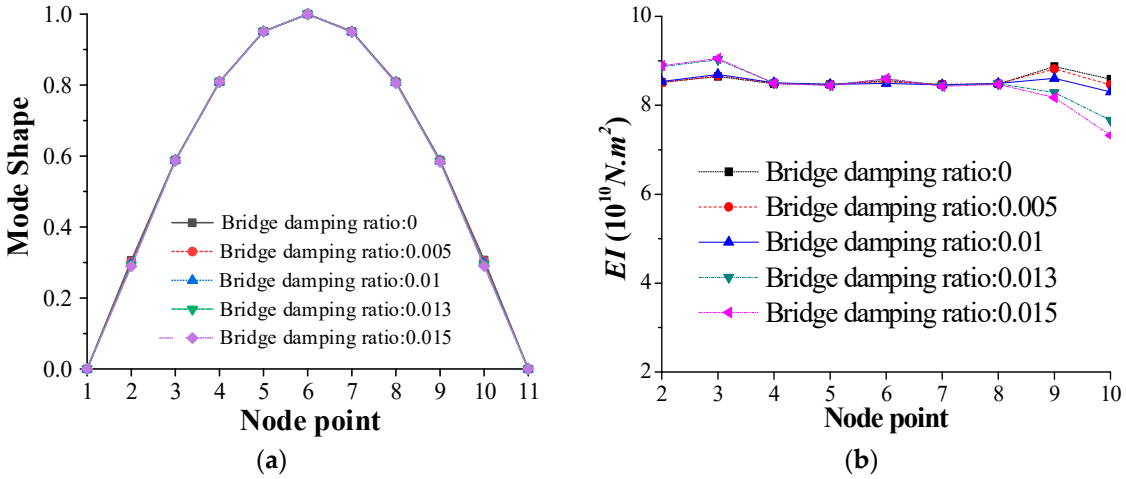

Figure 13. Contrast diagram of different damping ratios of the bridge with undamaged conditions for Class C of road surface roughness: (**a**) Mode shape; (**b**) Element bending stiffness *EI*.

3.7. Effect of Measurement Noise

Measurement noise will pollute the collected test data to a certain extent and affect the accuracy of the test. In this study, the signal-to-noise ratio (SNR), as defined below, is used to describe the effects of noise.

$$\mathrm{SNR} = 10 \times \lg \frac{\frac{1}{N}\sum_{i=1}^{N} y_i^2}{\frac{1}{N}\sum_{i=1}^{N} \sigma_i^2} \tag{38}$$

where N is the number of sampling time points at acceleration responses of the test vehicle, y_i is the acceleration response of the test vehicle containing noise at the i^{th} sampling time point, σ_i is the noise value at the i^{th} sampling time point, and SNR is the signal-to-noise ratio whose unit is db. It is noted that the SNR decreases when the noise level increases.

The simulations with the signal-to-noise ratio for each level are repeated 10 times to reduce the effects of random errors (similar to 10 insitu measurements). The average of the noise data is used to identified mode shape and corresponding *EI*. Based on the simulation model of Section 3 with consideration of Class C road surface roughness, the different signal-to-noise ratio is added to the acceleration recorded of the test vehicle, respectively. Figure 14 shows the results of the identified mode shape and identified *EI* with 20 db, 30 db, 40 dB, and 50 db, respectively.

All the identified mode shapes for the different signal-to-noise ratios are close to the theoretical one. The identified *EI* values at the bridge nodes differ slightly for different single-noise ratios. In Figure 14b, when the SNR is 50 db, the relative error of bending stiffness compared with the original *EI* is less than 3% for all bridge elements. When the SNR is 40 db, the relative error is less than 6%. Moreover, the bending stiffness can be reasonably identified even for up to 20 db and 30 db, and the relative error is less than 8% for all bridge elements.

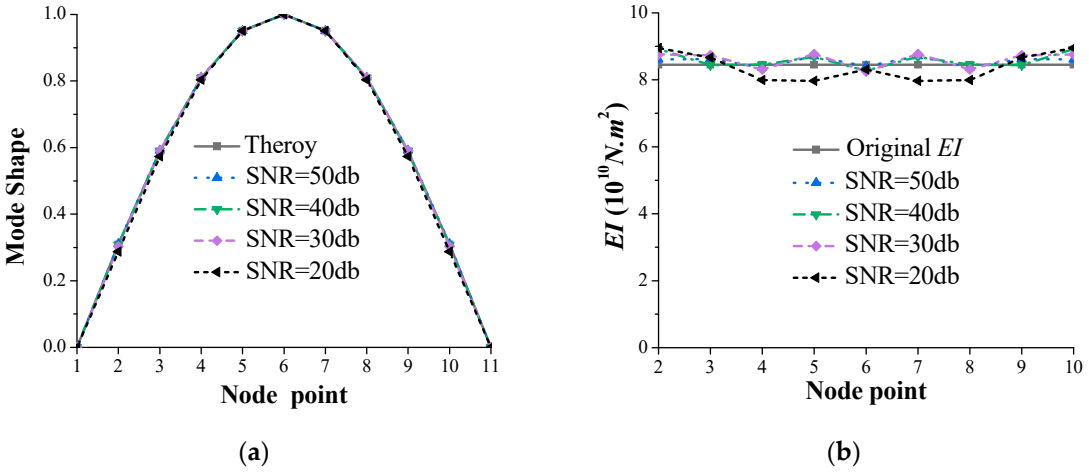

Figure 14. Identified results for different signal-to-noise ratio: (**a**) Mode shape; (**b**) Element bending stiffness *EI*.

4. Damage Scenarios Studied

Studies in the previous section show the features, accuracy, and limitations of the tractor-test vehicle technique of non-destructive testing in the stiffness identification of a simply-supported bridge deck. This section further studies the feasibility of this technique with different scenarios simulating cases of real application. The test vehicles in Table 1 and the bridge structure in Section 3 are adopted. The sensitivity of the tractor-test vehicle technique to the damping of the system and the road surface roughness is further studied in this section together with local damages in the system. Four different combinations of measurements are shown in Table 3 while the damage scenarios in each case are shown in Table 4. The finite element with local damage is referred to as D with a subscript denoting the element number. The assumed severity of the damage in an element is also shown in percentage.

Table 3. Vehicle-tractor-bridge system with different properties.

Cases	Vehicle	Bridge	Road Surface Roughness	Temperature (°C)
1	damped	undamped	--	-
2	damped	damped	--	-
3	damped	damped	Class C, D	-
4	damped	damped	Class C	-20, 0, 20 & 40

Table 4. Damage scenarios studied in each case.

Damage Scenario	Damage Element(s)	Related Node Numbers	Reduction in Element Stiffness (%)			
			(a)	(b)	(c)	(d)
A	D_2	2, 3	$D_2 = 0$	$D_2 = 15$	$D_2 = 30$	$D_2 = 50$
B	D_6	6, 7	$D_6 = 0$	$D_6 = 15$	$D_6 = 30$	$D_6 = 50$
C	D_4, D_7	4, 5 &7, 8	$D_4 = 0$ $D_7 = 0$	$D_4 = 15$ $D_7 = 15$	$D_4 = 30$ $D_7 = 30$	$D_4 = 50$ $D_7 = 50$
D	D_5, D_6	5, 6, 7	$D_5 = 0$ $D_6 = 0$	$D_5 = 15$ $D_6 = 15$	$D_5 = 30$ $D_6 = 30$	$D_5 = 50$ $D_6 = 50$

4.1. Case 1

Damped test vehiclesare passing through an undamped bridge with a smooth road surface. Theidentified 1st modal frequencyof the intact bridge deck is the same as the original frequency of 3.67 Hz, while there is a small reduction when there are local damages in each scenario studied.

The estimated mode shapes are shown in Figure 15 while the estimated element bending stiffness *EI* at the nodal points are shown in Figure 16. The mode shapes are close to each other for all the damage scenarios studied. The estimated bending stiffness *EI* shows clearly the location of local damage in different damage scenarios. The estimate on the damage severity in an element has a maximum relative error less than 5% at nodal point 3 in Scenario C with a 30% reduction in the stiffness of Elements 4 and 7. It is calculated as the mean of the stiffness values at two ends of the element. The estimated bending stiffness *EI* at the element nodal points are found independent of the value at other points which is consistent with previous observations [45], e.g., the estimated *EI* values are the same at node 7 in Scenarios 2, 3, and 4 and at node 5 in Scenarios 3 and 4. Results in Figure 13 also show the proposed improvement to the DSC method in Section 3 significantly reduces the boundary effect. The estimated *EI* values at nodes 2 and 10 are as good as those for the other nodes in all Scenarios with similar order of accuracy.

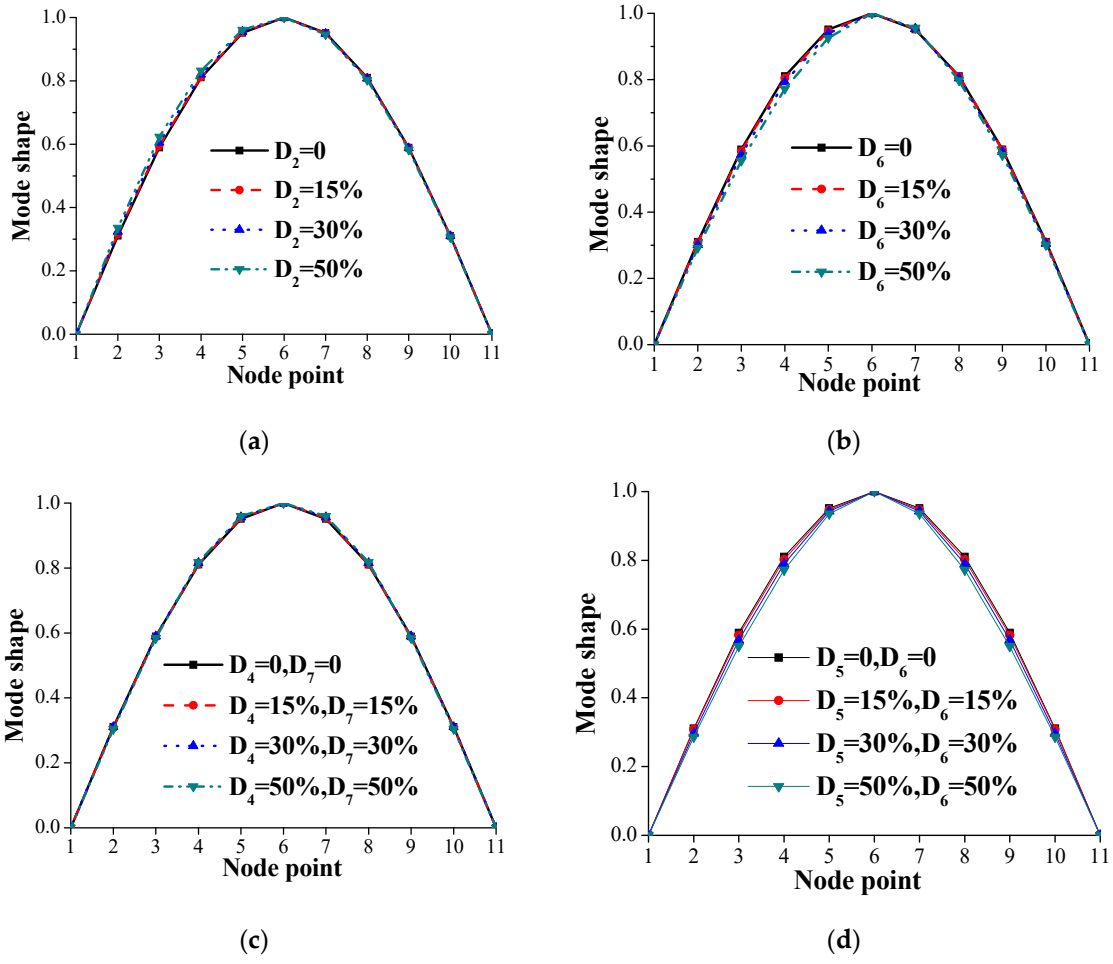

Figure 15. Estimated mode shape of undamped bridge for Case 1: (**a**) Scenario A; (**b**) Scenario B; (**c**) Scenario C; (**d**) Scenario D.

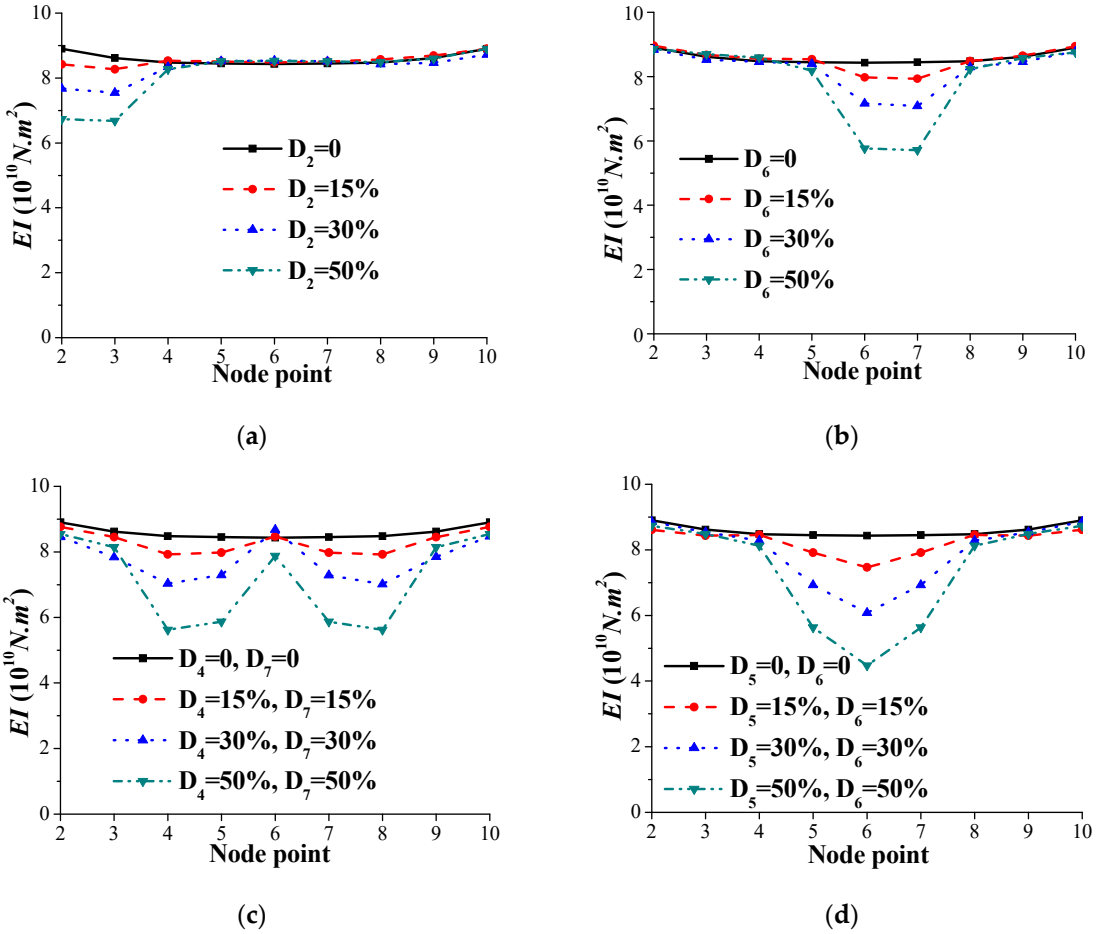

Figure 16. Estimated element bending stiffness *EI*ofthe undamped bridge for Case 1: (**a**) Scenario A; (**b**) Scenario B; (**c**) Scenario C; (**d**) Scenario D.

4.2. Case 2

A damping ratio $\xi_n = 0.01$ is included in the bridge model while the test vehicles are the same as those in the last study. The identified bridge modal frequencies are the same as those in Case 1. The estimated mode shapes are close to each other for all the scenarios studied. They are similar to those for Case 1 and therefore not shown.

The distributions of the estimated element bending stiffness *EI* shown in Figure 17 are similar to those for Case 1 with the maximum relative error less than 5% at nodal point 3 in Scenario C with a 30% reduction in the stiffness of Elements 4 and 7.

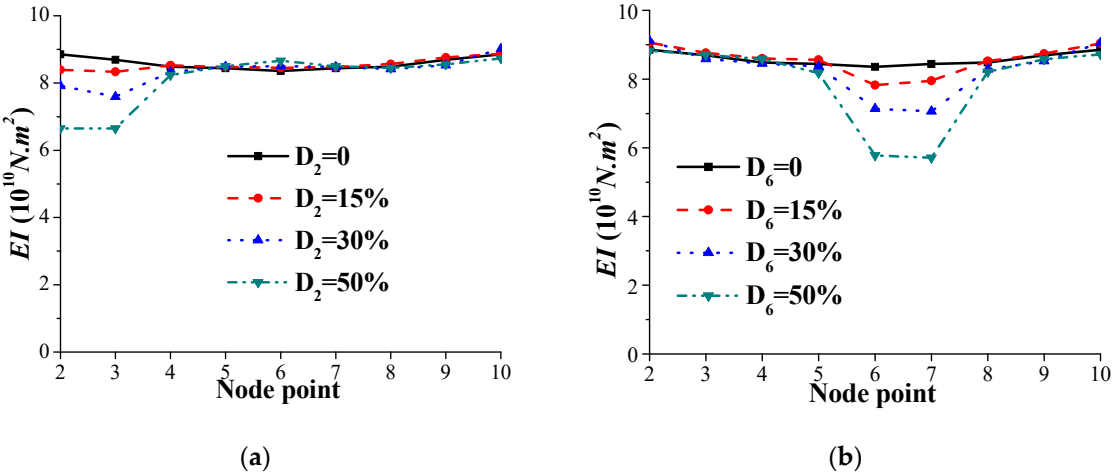

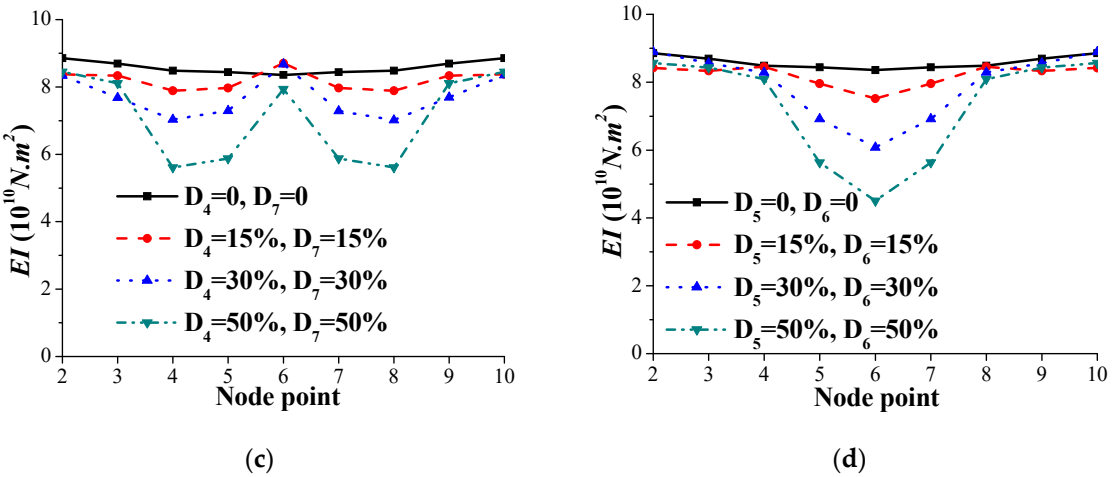

Figure 17. Estimated element bending stiffness *EI* of bridge for Case 2: (**a**) Scenario A; (**b**) Scenario B; (**c**) Scenario C; (**d**) Scenario D.

4.3. Case 3

The same vehicle-tractor-bridge system studied in the last section is adopted with additional Class C road surface roughness on the bridge deck. The identified bridge modal frequencies for all the scenarios studied are identical to those in the last study. The estimated mode shapes are similar to those in the last two cases and therefore not shown.

The element bending stiffness *EI* of the deck estimated from the identified bridge modal frequency and mode shape is shown in Figure 18. The boundary effect at the two ends of the structure becomes slightly larger compared to the last study. The estimated element bending stiffness *EI* are noted similar to those obtained in the last two studies with the maximum relative error of 11% in Element 10 in Scenario C.

When the road surface roughness is of Class D, i.e., $G_d(n_0)=1024\times10^{-6}\,\mathrm{m}^3$, the estimated element bending stiffness *EI* of the bridge deck shown in Figure 19 are noted acceptable except in Scenario A where the boundary effect affects seriously the identified results. The maximum relative error in the estimated element bending stiffness *EI* occurs in Element 10 of Scenario B with 50% reduction in the stiffness of element 6 with a value of approximately 16%.

It may be concluded that when the road surface roughness is high as in Class D, the boundary effect in the identification couples with the road surface roughness effect leading to unsatisfactory identified results close to the end of the bridge deck while the remaining results are acceptable for the damage identification.

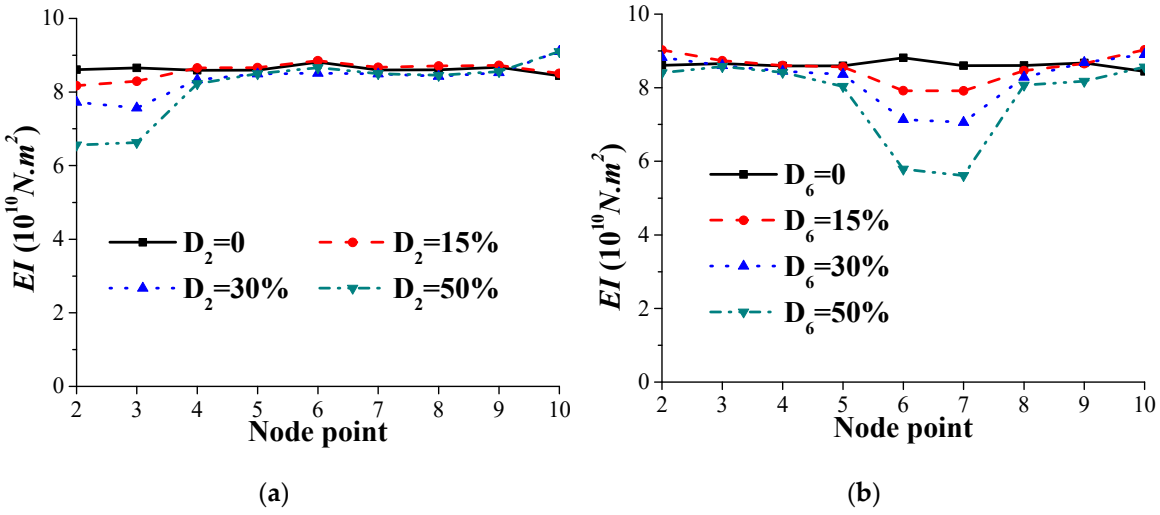

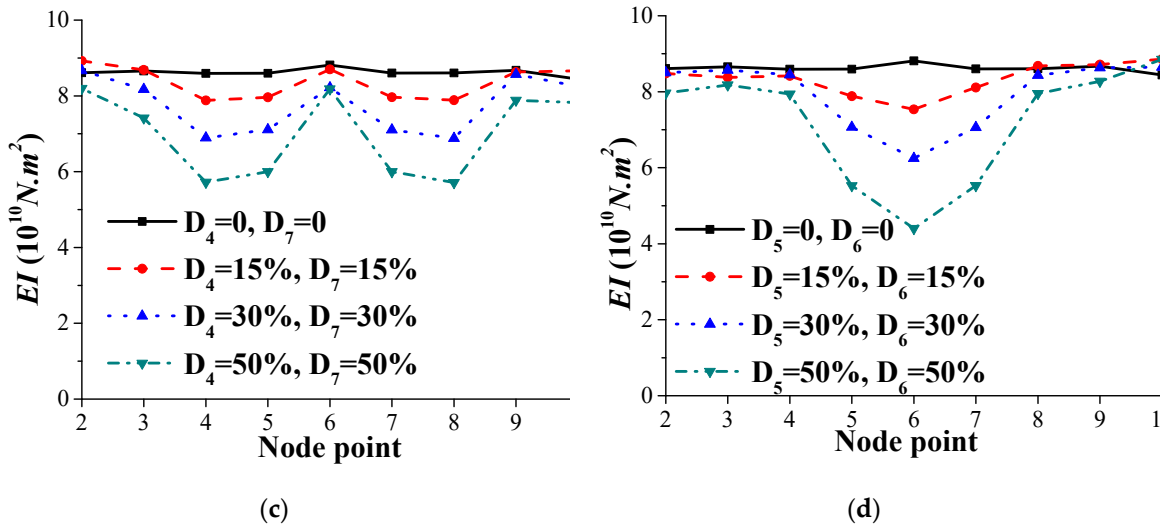

Figure 18. Estimated element bending stiffness *EI* of the bridge for Case 3 with Class C road surface roughness: (**a**) Scenario A; (**b**) Scenario B; (**c**) Scenario C; (**d**) Scenario D.

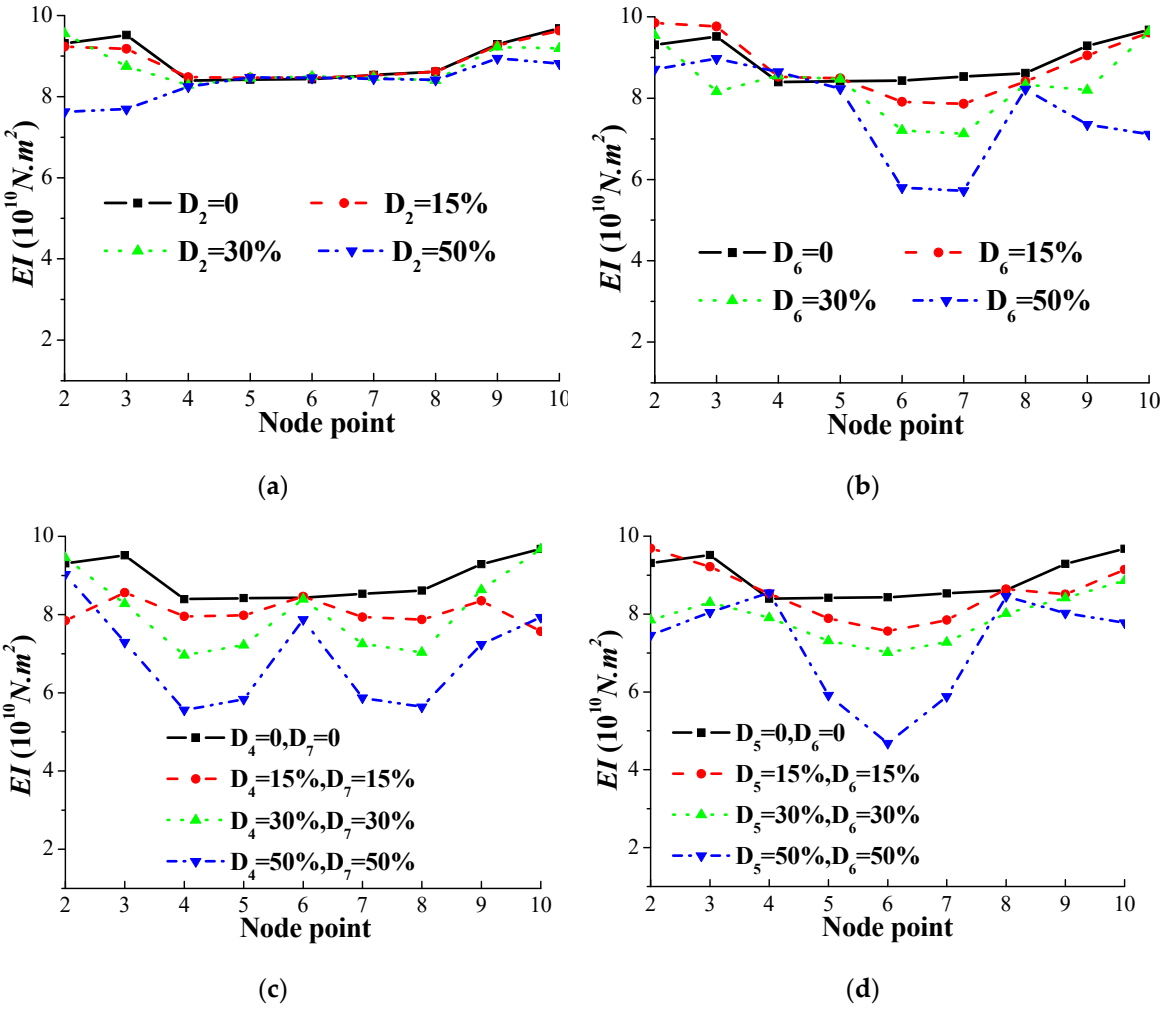

Figure 19. Estimated element bending stiffness *EI* of the bridge for Case 3 with Class D road surface roughness: (**a**) Scenario A; (**b**) Scenario B; (**c**) Scenario C; (**d**) Scenario D.

4.4. Case 4

Considering the road surface roughness is of Class C, the last study is repeated in this section with different ambient temperatures in the measurements. The elastic modulus of the material is assumed associated with the ambient temperature of 7 °C in the first round of measurement. The ambient temperature of the second round of measurement is assumed at –20, 0, 20, and 40 °C in turn in this study, and the corresponding identified 1st modal frequencies of the intact bridge are 3.833 Hz, 3.733 Hz, 3.567 Hz, and 3.467 Hz, respectively. The corresponding mode shapes are shown overlapping with each other in Figure 20. This indicates measurements at different ambient temperatures do not have any influence on the identified mode shape.

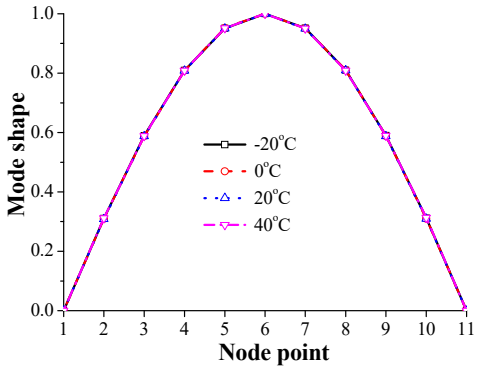

Figure 20. 1st vibration mode shape of the intact bridge at different ambient temperatures.

The identified modal frequency of the deck structure is adjusted to correspond to the reference temperature of 20 °C, while the identified mode shape is kept. The estimated element bending stiffness *EI* for the intact bridge shown in Figure 21 is close to the true values with a maximum error less than 6% at the end nodal point 10 due to the boundary effect of the improved DSC method.

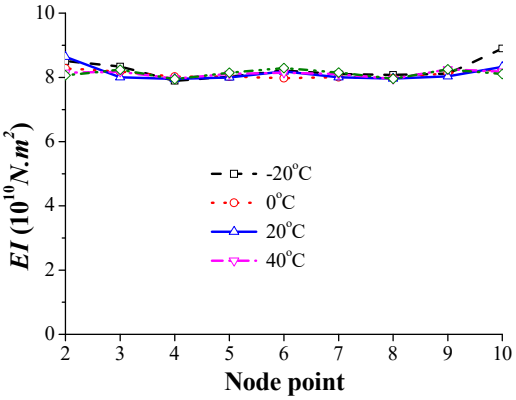

Figure 21. Estimated element bending stiffness *EI* from measurements at different ambient temperature.

The four damage scenarios with a 30% reduction in the element stiffness are studied further in this section. With the adjustment and procedure similar to that for the intact bridge deck above, and the estimated element bending stiffness *EI* for the deck is shown in Figure 22. The estimates are noted similar to those in Figure 17 with a maximum relative error less than 9% at the end nodes.

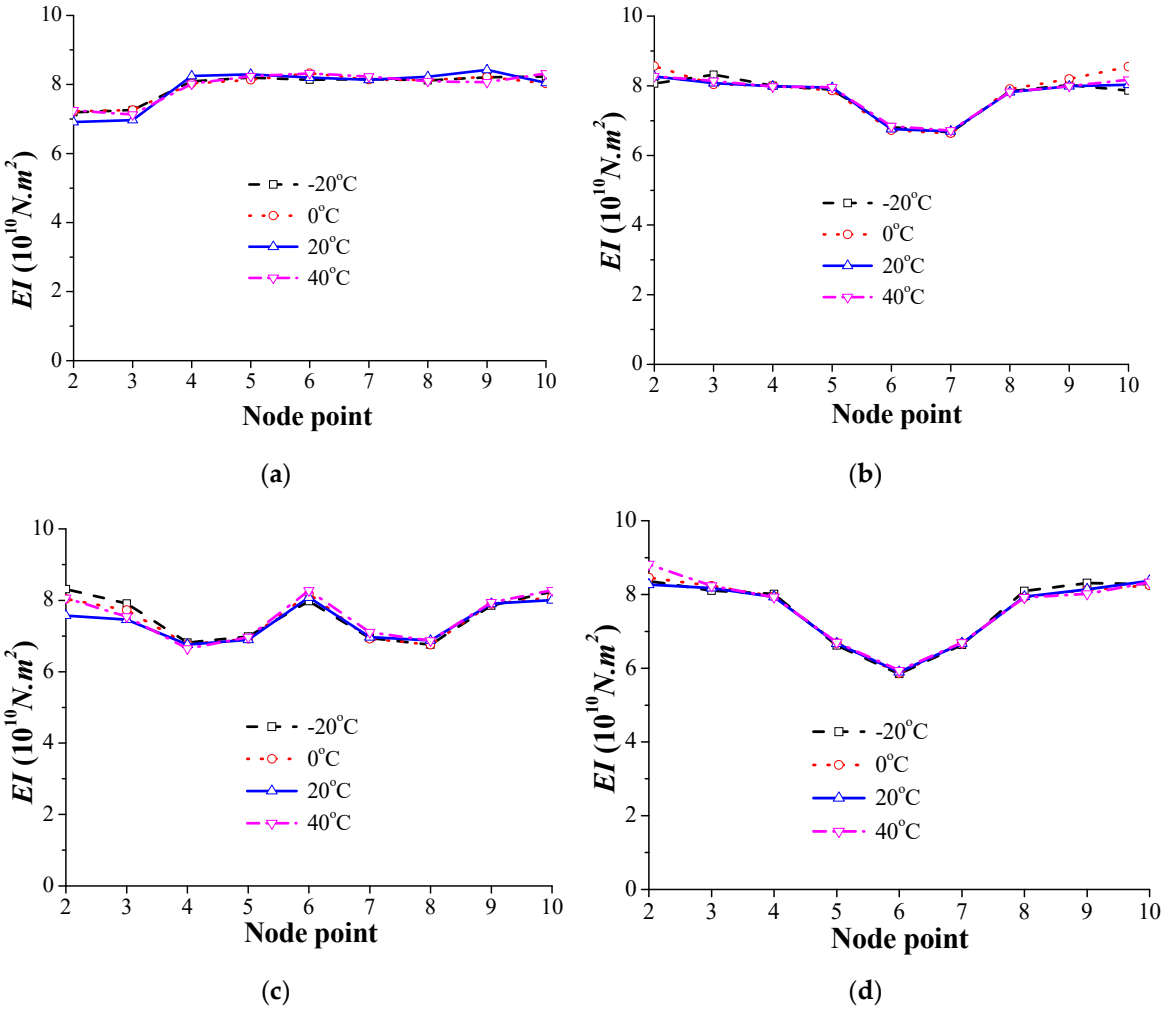

Figure 22. Identified element bending stiffness *EI* from measurements at different ambient temperatures: (**a**) Scenario A, D_2 = 30%; (**b**) Scenario B, D_6 = 30%; (**c**) Scenario C, D_4 = 30% and D_7 = 30%; (**d**) Scenario D, D_5 = 30% and D_6 = 30%.

Based on the simulation model above, undamaged scenario and Scenario C with SNR = 30 db, ambient temperature at 0 °C,and non-constant vehicle speed from 0.9875 m/s to 1.0125 m/s randomly are chosen for combining effect analysis. With the aboveanalysis procedure in Section 2.5, and the estimated element bending stiffness *EI* is shown in Figure 23. The estimates are similar to those in Figures 21 and 22 with a maximum relative error less than 10% at the end nodes.

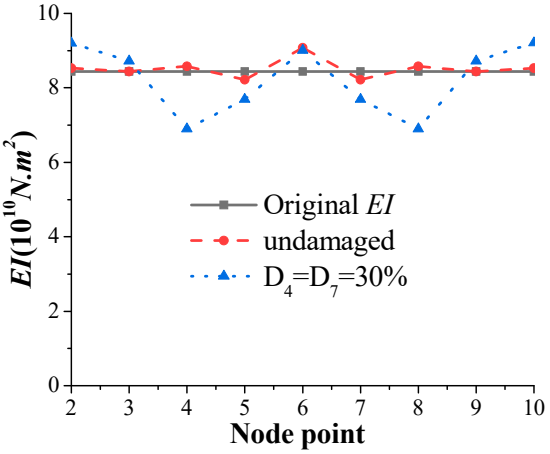

Figure 23. Identified element bending stiffness *EI* from the combined effect analysis: (**a**) undamaged scenario; (**b**) Scenario C, D_4 = 30% and D_7 = 30%.

4.5. Discussion on the Boundary Effects

Figures 13, 15, 18 and 19 shows that the boundary effect is consistently high in the estimated element bending stiffness *EI*. It is noted that the discretization error in the finite element modeling of the beam structure may also affect the estimation. Another study is conducted in this section with 25% of the length of the beam finite element close to the end node of the beam further sub-divided into smaller finite elements in the structural model.

The identified results for Scenario B with a 50% reduction in the stiffness of Element 6 are shown in Figure 24. The relative error at the nodes closest to the end nodes 2 and 10 have been reduced significantly from 16% in Figure 19b to 11% in Figure 24. Since the estimates are noted independent of adjacent values, the proposed approach is considered applicable to identify stiffness of the deck except at a small region close to the simply supported ends with acceptable accuracy.

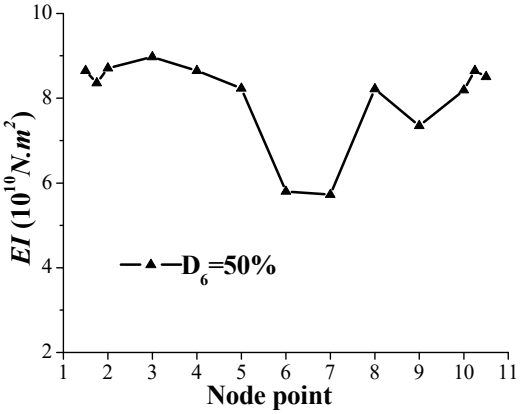

Figure 24. Estimated element bending stiffness *EI* with refined finite element close to the boundary

4.6. Discussion on the Variation of Bridge Bearing

The damage form of bridge studied in the above mentioned is the reduction of bending stiffness of bridge elements. However, in practice, the damage of bridge bearings is also one of the common phenomena of bridge damage. The damage of bridge bearings is often reflected in the reduction of the vertical stiffness of bridge bearings. Therefore, this section studies the feasibility of this method for bearing damage identification.

The two ends of the simply supported beam are replaced by springs with a stiffness coefficient of $k = 1.6 \times 10^{10} N/m$ with consideration of rubber bearing. Figure 25 shows the 1st mode shape and bending stiffness of the beam identified by the procedure of Figure 3. It can be seen that the identified value is very close to the theoretical value in the undamaged state without the reduction of the vertical stiffness of bridge bearing. When the bearing vertical stiffness of the left side support of the beam reduced by 10%, 30%, 50%, respectively, the identified 1st mode shape and bending stiffness results are also shown in Figure 25. It indicated that the identified left side boundary element bending stiffness decreased with the increased damage level of the bearing vertical stiffness. It is significant of showing that the technique is also suitable for identifying the damage of the bridge bearing without consideration of boundary element stiffness reduction.

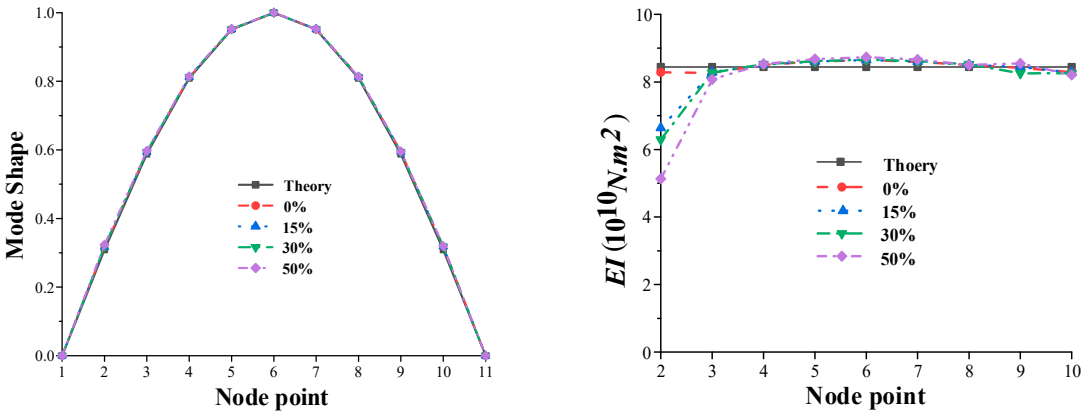

(**a**) (**b**)

Figure 25. Identified results for different left bearing stiffness reduction: (**a**) Mode shape and; (**b**)element bending stiffness *EI*.

5. Field Test Study

The Li ziwan Bridge, located in Fu ling District of Chongqing City, is a six-span prestressedconcrete bridge constructed in 1990 and reinforced in 2011, as shown in Figure 26, which is a simply-supported girder bridge with the length of 196m and the width of 12m. The single-span bridge is made of six prestressed-concrete hollow slabs and 30m in length. The cross-sectional moment of inertia is 0.79 m^4, and the elastic modulus is 3.25×10^{10} N/m^2. The cross-section of the bridge has a total width of 12m with 12 hollow slabs, as shown in Figure 27. The bridge consists of two lanes in each direction and serves traffic with a maximum speed of 30 km/h. The traffic flow on the bridge is very limited due to its remote location so that although not newly built, it is still structurally sound and ingood condition.

The data acquisition system used in this field experiment mainly includes vibration sensors and a data acquisition device.The sensor is a strain acceleration sensor produced by Lance Test Technology Co., Ltd. as shown in Figure 28a, which has a maximum sampling frequency of 2500 Hz. The TST5912 dynamic signal test analysis system produced by Jiangsu Test Electronic Equipment Manufacturing Co., Ltd. was adopted as the data acquisition device, as shown in Figure 28b.

(**a**) (**b**)

Figure 26. Li ziwan Bridge of Chongqing City: (**a**) Upper surface; (**b**) Lower surface.

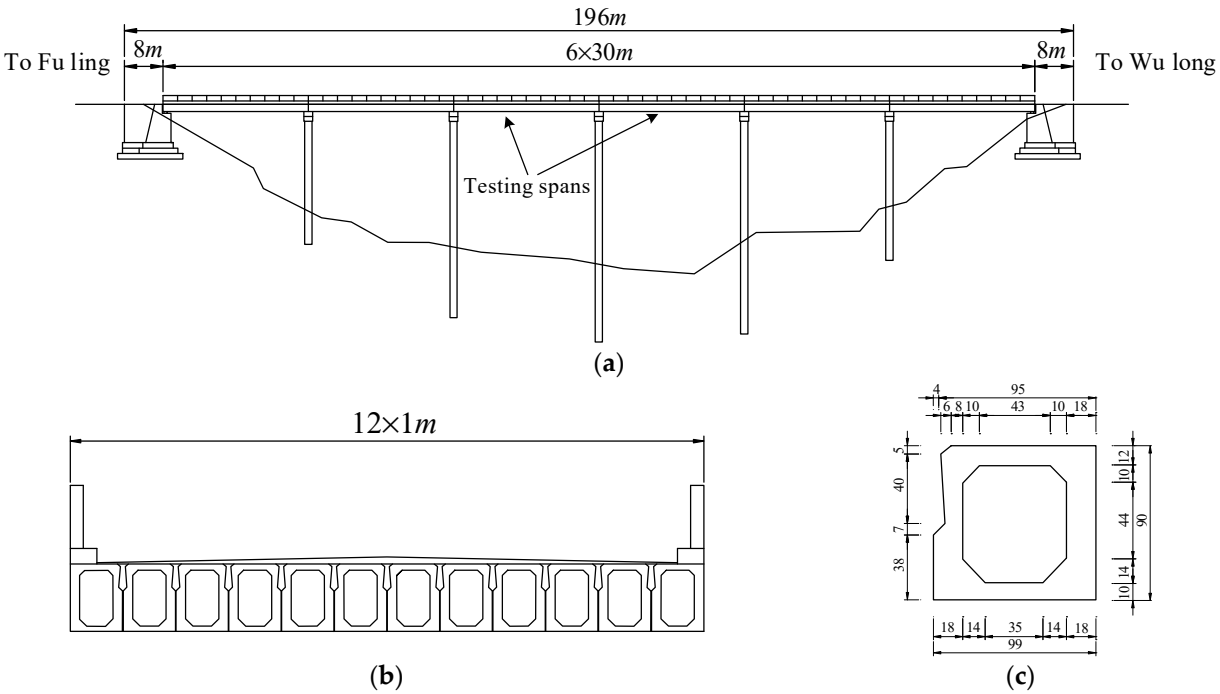

Figure 27. Testingbridge: (**a**) Bridge elevation; (**b**) Bridge cross-section; (**c**) Girder cross-section.

Figure 28. (**a**) Accelerometer; (**b**) Data acquisition device.

The vibration transducer was used only in the middle of the testing span (the 4th and 3rd spans shown in Figure 27a) for the ambient vibration test.The test method for the 4th and 3rd spans is the same, so the data of the 4th span measurement is mainly shown below.The total length of each record is 60s with a sampling rate of 100 Hz. To determine the exact fundamental bridge frequency and 1st damping ratio, the testing span of the bridge was recorded 5 times with an intervalof 10 min. Figure 29 shows the Fast Fourier Transform (FFT) of one recorded data at the testing spanof the bridge, from which the peaks associated with the dominant frequencies of the bridge are identified. The fundamental bridge frequency can be identified as 3.71 Hz, and the 1st damping ratio can be calculated by stochastic subspace identification (SSI)method, which is 0.0077.Considering the bridge construction drawing and field test, the original *EI* value of the deck is calculated as $2.57\times10^{10}N\cdot m^2$.

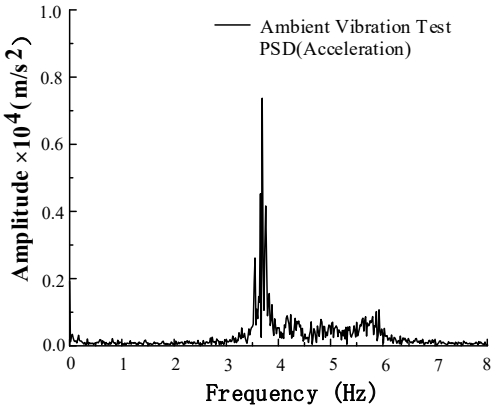

Figure 29. Power spectral density of ambient vibration acceleration record of the 4th span.

The tractor-test vehicle system used for measurement is two specialized vehicles consisting of a tractor and a following test vehicle, as shown in Figure 30. The following test vehicle is a single-axle vehicle with a weight of 1.482 tons (similar to No.2 test vehicle) or 0.988 tons (similar to No.1 test vehicle), towed across the bridge by a tractor, which is a four-wheel commercial light truck of 3.025 tons with a wheel spacing of 2.025 m. Figure 31 shows that the parameters of the test vehicle are tested by a micro-vibration experiment on a shaking table. According to the results, it is known that the modal frequency and damping ratio of the two test vehicles are 2.84 Hz and 0.066, respectively..

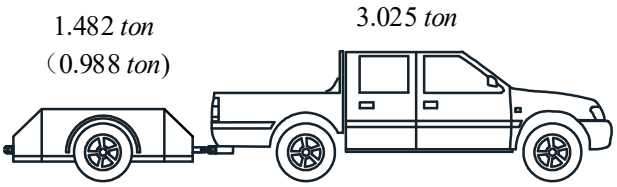

Figure 30. Thetractor-test vehicle system.

Figure 31. The single-axletest vehicleis tested on a shaking table.

Considering the testing spans, researchers kept the speed of the tractor-test vehicle system at 1m/s, as shown in Figure 32. According to the test vehicle going across the testing span of the bridge, the acceleration response of the test vehicle with an acceleration sensor installed in the center of gravityof the test vehicle could be recorded and then transmitted to the remote computer platform for analysis. For reducing the effect of the road surface roughness, two test vehicles with different weights, namely big test vehicle (1482 kg) and small test vehicle (988 kg) with the same vehicle frequencyand vehicle damping ratio, could pass the testing spans of the bridgeat a speed of 1m/s under the pull of the tractorrespectively,Figure 33 shows the acceleration response of test vehicleswhen the test vehicle passes the 4th span. Then, under the initial condition of zero, the displacement response can be obtained by integrating the acceleration twice.The residual displacement response is obtained by subtracting the displacement response of the two test vehicles, which will be used to obtain the residual acceleration response by taking the second derivatives, namely $\Delta\ddot{u}(t)$ as mentioned in the Analysis Procedure at Section 2.5. Figure 34 shows the

residualacceleration response and the fast Fourier transform (FFT) of the residual acceleration response,which indicates clearly that the residual acceleration signals can identify the fundamental bridge frequency.

Figure 32. Field test on site.

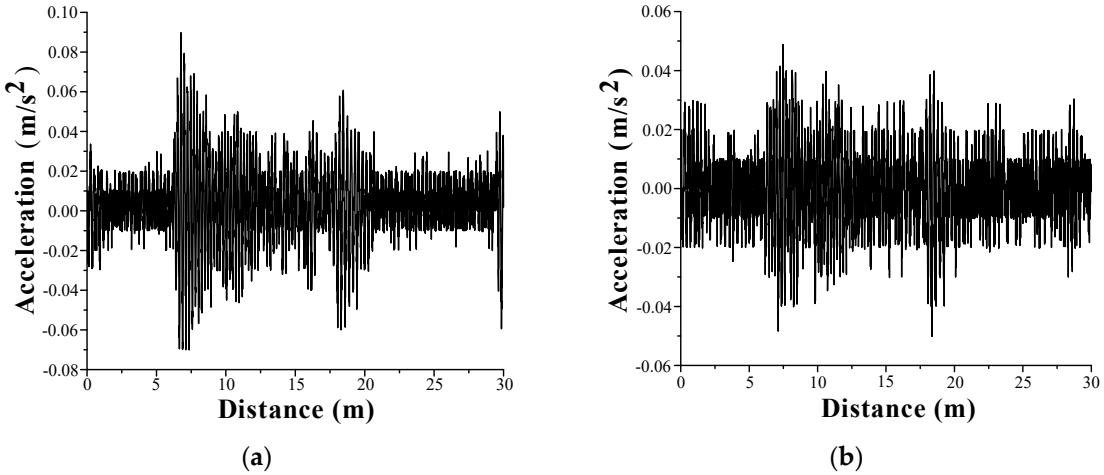

Figure 33. The acceleration response of: (**a**) big test vehicle; (**b**) small test vehicle.

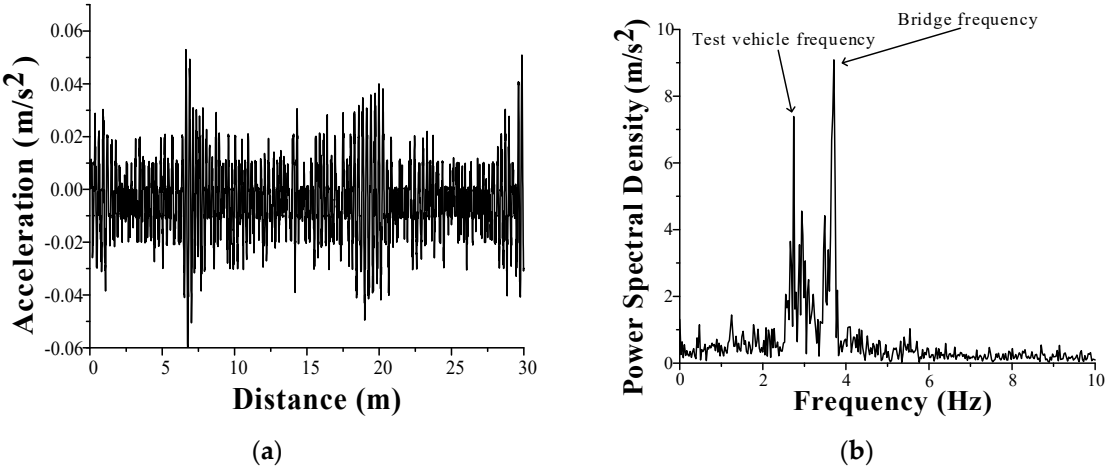

Figure 34. (**a**) Time history and; (**b**) Power spectral density of the residual acceleration signals.

Based on the analysis procedure in Section 2.5, the 1st mode shape and estimated element bending stiffness *EI* of the 4th and 3rd spans are plotted in Figures 35 and 36, respectively. Whether on the 4th or 3rd span, there is no obvious difference between the mode shapes. Compared with the original *EI*, the maximum relative error in the identified stiffness *EI* occurs in node numbers 10 and 9 with a value of approximately 17% and 19%, respectively, due to boundary zero modal value effectand the remaining *EI* results are all below 16%. This can be accepted within an engineering acceptance range. The weight of the test vehicle and tractor is applied as a load on the bridge deck. When the tractor and following test vehiclesare driven to the mid-span, the mid-span relative

deflection of the bridge adding the weight of the tractor and test vehicles can be calculated by the identified bending stiffness, which is consistent with the measurement results by using the total station.

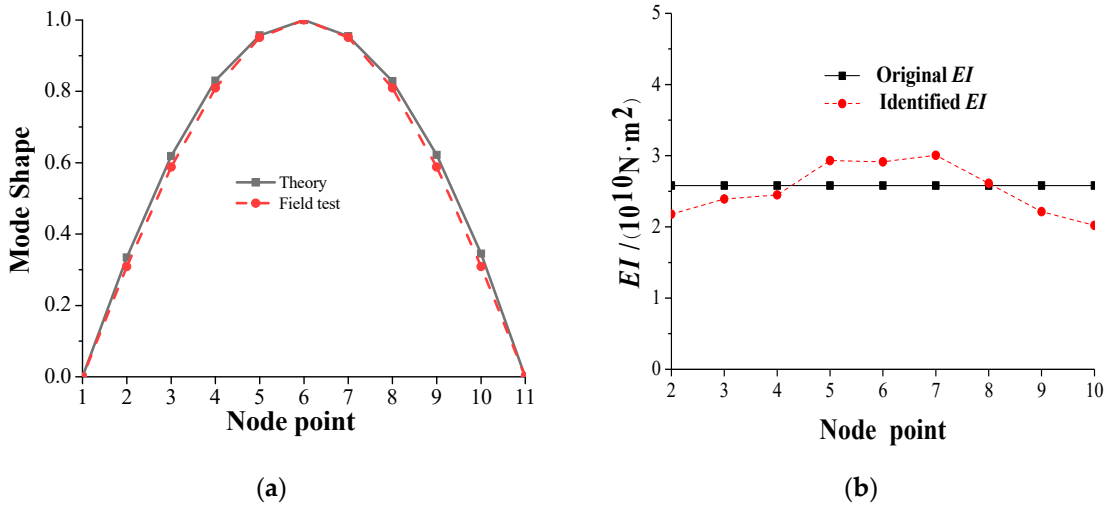

Figure 35. Identified results of the 4thspan for field test: (**a**) Mode shape; (**b**) Bending stiffness *EI*.

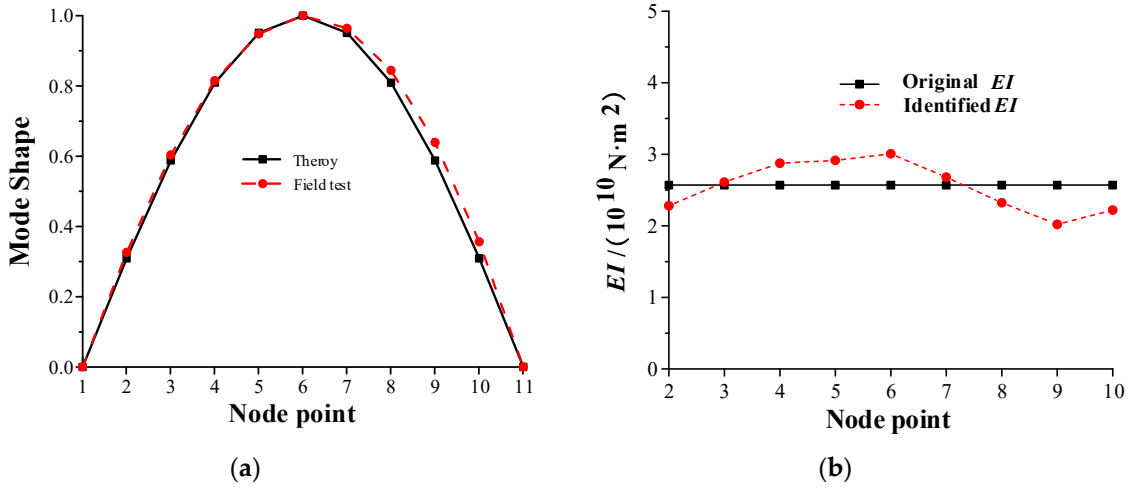

Figure 36. Identified results of the 3rdspan for field test: (**a**) Mode shape; (**b**) Bending stiffness *EI*.

6. Conclusions

The feasibility of the tractor-test vehicle technique of non-destructive testing for practical application is studied. Only the modal properties of the first vibration mode of the bridge are required in the proposed method. Different damage scenarios are studied with the vehicle-tractor-bridge system. The following conclusions may be drawn:

(1) Two test vehicles are designed to have identical modal frequency and damping ratio, but the No.2 test vehicle has a mass, stiffness and damping coefficient proportional to those of the No.1 test vehicle. This technique can help to generate a response from an equivalent vehicle of a single vehicle-bridge system that is free from the effect of road surface roughness.

(2) The first modal frequency and mode shape of the deck structure can be accurately estimated from the response of the equivalent vehicle with consideration of damping of the vehicle-tractor-bridge system, non-uniform test vehicle speed, measurement noise, and different ambient temperatures in the measurements.

(3) The bending stiffness *EI* of the bridge deck can be better estimated with improvements proposed for the DSC method. For locations such as simply-supported ends of the beam, the improved DSC method can be used to obtain the stiffness by extrapolating the mode shape and using a

refined model (or denser data measurements) near these locations.

(4) The tractor-test vehicle technique of non-destructive testing with the proposed modifications has been demonstrated to be feasible for practical application to regular monitoring and evaluation of the structural health condition of a beam-like bridge deck with the advantages of simplicity, mobility, and ease of implementation.

Author Contributions: Conceptualization, Y.Y.; Methodology, Y.Z.; Formal analysis, L.W.; Data curation, R.J.; Writing—original draft preparation, Q.C.; Writing—review and editing, Y.Y. All authors have read and agreed to the published version of the manuscript.

Funding: This study was supported by the following agencies: National Natural Science Foundation of China (Grant No. 51778090, 5191153024), Science and technology plan project of Chongqing Science and Technology Bure (Project No. cstc2019jscx-msxmX0015), Graduate research and innovation Foundation of Chongqing, China (Grant No.CYS19004), Fu Ling District Science and Technology Plan Project (FLKJ 2018BBA3038).

Acknowledgments: We would like to thank Hao bin, director of Chongqing Chang An Automobile Research Institute, for his help in the design of the test vehicle.

Conflicts of Interest: The authors declare no conflict of interest.

References

1. Yang, Y.; Mosalam, K.M.; Liu, G.; Wang, X.L. Damage detection using improved direct stiffness calculations-a case study. *Int. J. Struct. Stab. Dyn.* **2016**, *16*, 1640002.
2. Kim, S.; Oberheim, T.; Pakzad, S.; Fenves, G. *Structural Health Monitoring of the Golden Gate Bridge*; UC Berkeley Nest Retreat Presentation Jan: Berkeley, CA, USA, 2003; pp. 223–243.
3. Chan, T.H.; Yu, L.; Tam, H.Y.; Ni,Y.Q.; Liu, S.Y.; Chung, W.H. Fiber Bragg grating sensors for structural health monitoring of Tsing Ma bridge: Background and experimental observation. *Eng. Struct.* **2006**, *28*, 648–659.
4. Yang, Y.; Yang, L.; Wu, B.; Yao, G.; Li, H.; Robert, S. Safety prediction using vehicle safety evaluation model passing on long-span bridge with fully connected neural network. *Adv. Civ. Eng.* **2019**, *2019*, 8130240.
5. Yang, Y.B.; Lin, C.W.; Yau, J.D. Extracting bridge frequencies from the dynamic response of a passing vehicle. *J. Sound Vib.* **2004**, *272*, 471–493.
6. Lin, C.W.; Yang, Y.B. Use of a passing vehicle to scan the fundamental bridge frequencies: An experimental verification. *Eng. Struct.* **2005**, *27*, 18651–18878.
7. Yang, Y.B.; Chen, W.F.; Yu, H.W.; Chan, C.S. Experimental study of a hand-drawn cart for measuring the bridge frequencies. *Eng. Struct.* **2013**, *57*, 2222–2231.
8. Yang, Y.B.; Chen, W.F. Extraction of bridge frequencies from a moving test vehicle by stochastic subspace identification. *J. Bridge Eng.* **2016**, *21*, 4015053.
9. Yang, Y.B., Li, Y.C.; Chang, K. Constructing the mode shapes of a bridge from a passing vehicle: A theoretical study. *Smart Struct. Syst.* **2014**, *13*, 7978–7919.
10. Malekjafarian, A.; Obrien, E.J. On the use of a passing vehicle for the estimation of bridge mode shapes.*J. Sound Vib.* **2017**, *397*, 77–91.
11. Malekjafarian, A.; Obrien, E.J. Identification of bridge mode shapes using Short Time Frequency Domain Decomposition of the responses measured in a passing vehicle. *Eng. Struct.* **2014**, *81*, 386–397.
12. Gomeza, H.C.; Fanning, P.J.; Feng, M.Q.; Lee, S. Testing and long-term monitoring of a curved concrete box girder bridge. *Eng. Struct.* **2011**, *33*, 2861–2869.
13. Kim, J.; Lynch, J.P. Experimental analysis of vehicle–bridge interaction using a wireless monitoring system and a two-stage system identification technique. *Mech. Syst. Signal Process.* **2012**, *28*, 31–39.
14. Siringoringo, D.M.; Fujino, Y. Estimating bridge fundamental frequency from vibration response of instrumented passing vehicle: Analytical and experimental study. *Adv. Struct. Eng.* **2012**, *15*, 417–433.
15. Sitton, J.D.;Zeinali, Y.; Story, B.A. Frequency Estimation onTwo-Span Continuous Bridges Using Dynamic Responses of PassingVehicles. *J. Eng. Mech.* **2020**, *146*, 4019115.
16. Gonzalez, A.; OBrien, E.J.; McGetrick, P.J. Identification of damping in a bridge using a moving instrumented vehicle. *J. Sound Vib.* **2012**, *331*, 4115–4131.
17. Keenahan, J.; Obrien, E.J.; McGetrick, P.J.; González, A. The use of a dynamic truck-trailer drive-by system to monitor bridge damping. *Struct. Health Monit.* **2014**, *13*, 143–157.
18. Yang, Y.B.; Zhang, B.; Chen, Y.N.; Qian, Y.; Wu, Y.T. Bridge damping identification by vehicle scanning method. *Eng. Struct.* **2019**, *183*, 637–645.
19. Chang, K.C.; Wu, F.B.; Yang, Y.B. Effect of road roughness on indirect approach for measuring bridge

frequencies form a passing vehicle. *Interact. Multiscale Mech.* **2010**, *3*, 299–308.
20. Yang, Y.B.; Li, Y.C.; Chang, K.C. Using two connected vehicles to measure the frequencies of bridges with rough surface: A theoretical study. *Acta Mech.* **2012**, *223*, 1851–1861.
21. Kong, X.; Cai, C.S.; Kong, B. Numerically Extracting Bridge Modal Properties from Dynamic Responses of Moving Vehicles. *J. Eng. Mech.* **2016**, *142*, 4016025.
22. Bu, J.Q.; Law, S.S.; Zhu, X.Q. Innovative bridge condition assessment from dynamic response of a passing vehicle. *J. Eng. Mech.* **2006**, *132*, 1372–1379.
23. Kim, C.W.; Kawatani, M. Pseudo-static approach for damage identification of bridges based on coupling vibration with a moving vehicle. *Struct. Infrastruct. Eng.* **2008**, *4*, 371–379.
24. Yin, S.S.; Tang, C.Y. Identifying cable tension loss and deck damage in a cable-stayed bridge using a moving vehicle. *J. Vib. Acoust.* **2011**, *133*, 898–923.
25. Lu, Z.R.; Liu, J.K. Identification of both structural damages in bridge deck and vehicle parameters using measured dynamic response. *Comput. Struct.* **2011**, *89*, 1397–1405.
26. Miyamoto, A.; Yabe, A. Bridge condition assessment based on vibration response of passenger vehicle.*J. Phys.* **2011**, *305*, 1–10.
27. Zhang, Y.; Lie, S.T.; Xiang, Z.H. Damage detection method based on operating deflection shape curvature extracted from dynamic response of a passing vehicle. *Mech. Syst. Signal Process.* **2013**, *35*, 238–254.
28. Zhang, Y.; Wang, L.Q.; Xiang, Z.H. Damage detection by mode shape squares extracted from a passing vehicle.*J. Sound Vib.* **2012**, *331*, 291–307.
29. Li, Z.; Au, F.T.K. Damage detection of bridges using response of vehicle considering road surface roughness. *Int. J. Struct. Stab. Dyn.* **2015**, *15*, 1450057.
30. Feng, D.M.; Feng, M.Q. Output-only damage detection using vehicle-induced displacement response and mode shape curvature index. *Struct. Control. Health Monit.* **2016**, *23*, 1088–1107.
31. Mei, Q.; Gul, M.; Boay, M. Indirect health monitoring ofbridges using Mel-frequency cepstral coefficients and principal componentanalysis. *Mech. Syst. Signal Process.* **2019**, *119*, 523–546.
32. Yang, Y.; Zhu, Y.H.; Wang, L.L.; Jia, B.Y.L.; Jin, R.Y. Structural Damage identification of bridges from passing test vehicles. *Sensors*. **2018**, *18*, 4035.
33. Shi, Z.Y.; Law, S.S.; Zhang, L.M. Improved damage quantification from elemental modal strain energy change. *J. Eng. Mech.* **2002**, *128*, 521–529.
34. Kim, B.S.; Yoo, S.H.; Yeo, G.H. Characterization of crack detection on gusset plates using strain mode shapes. In Proceedings of the 23rd International Modal Analysis Conference (IMAC XXIII), Orlando, FL, USA, 31 January 31–3 February 2005.
35. Li, J.; Law, S.S.; Ding, Y. Substructure damage identification based on response reconstruction in frequency domain and model updating. *Eng. Struct.* **2012**, *41*, 270–284.
36. Zhong, H.; Yang, M.J. Damage detection for plate-like structures using generalized curvature mode shape method. *J. Civ. Struct. Health Monit.* **2016**, *6*, 141–152.
37. Samami, H.; Oyadiji, S.O. Simulation and detection of small crack-like surface flaws and slots in simply-supported beams using curvature analysis of analytical and numerical modal displacement data. *Eng. Comput.* **2016**, *33*, 1969–2006.
38. Yang, Y.; Li, J.L.; Zhou, C.H.; Law, S.S.; Lv, L. Damage detection of structures with parametric uncertainties based on fusion of statistical moments. *J. Sound Vib*. **2019**, *442*,200–219.
39. OBrien, E.J.; McGetrick, P.J.; Gonzalez, A. A drive-by inspection system via vehicle moving force identification. *Smart Struct. Syst.* **2014**, *13*, 821–848.
40. Dao, P.B.; Staszewski, W.J.; Klepka, A. Stationarity-based approach for the selection of lag length in cointegration analysis used for structural damage detection. *Comput. Aided Civ. Infrastruct. Eng.* **2017**, *32*, 138–153.
41. Niemann, H.; Morlier, J.; Shahdin, A.; Gourinat, Y. Damage localization using experimental modal parameters and topology optimization. *Mech. Syst. Signal Process.* **2010**, *24*, 636–652.
42. Li, W.M.; Jiang, Z.H.; Wang, T.L.; Zhu, H.P. Optimization method based on generalized pattern search algorithm to identify bridge parameters indirectly by a passing vehicle. *J. Sound Vib.* **2014**, *333*, 364–380.
43. Maeck, J. Damage Assessment of Civil Engineering Structure by Vibration Moanitoring. Ph.D.Thesis, Department of Civil Engineering, KatholiekeUniversiteit Leuven, Brussels, Belgium, 2003.
44. Huth, O.; Feltrin, G.; Maeck, J.; Kilic, N.; Motavalli, M. Damage identification using modal data: Experiences on a prestressed concrete bridge. *J. Struct. Eng.* **2005**, *131*, 1898–1910.
45. Yang, Y.; Liu, H.; Mosalam, K.M.; Huang, S.N. An improved direct stiffness calculation method for damage detection of beam structures. *Struct. Control Health Monit.* **2013**, *20*, 835–851.
46. Wang, L.H. Studies on Non-Destructive Damage Detection of Bridges Based on Linear and Nonlinear Dynamic Characteristics. Ph.D.Thesis, College of Architecture, Civil Engineering, Beijing University of

Technology, Beijing, China, 2006.
47. Yang, Y.; Yang, Y.B.; Chen, Z.X. Seismic damage assessment of RC structures under shaking table tests using the modified direct stiffness calculation method. *Eng. Struct.* **2017**, *131*, 545–586.
48. Yau, J.D.; Yang, Y.B.; Kuo, S.R. Impact response of high-speed rail bridges and riding comfort of rail car. *Eng. Struct.* **1999**, *21*, 836–844.
49. Yau, J.D.; Yang, J.P.; Yang, Y.B. Wavenumber-based technique for detecting slope discontinuity in simple beams using moving test vehicle. *Int. J. Struct. Stab. Dyn.* **2017**, *17*, 1750060.
50. ISO 8608. *Mechanical Vibration-Road Surface Profiles—Reporting of Measured Data*; ISO: Geneva, Switzerland, 1995.
51. Gu, J.F.; Gul, M.; Wu, X.G. Damage detection under varying temperature using artificial neutral networks. *Struct. Control Health Monit.* **2017**, *24*, 1998.
52. Hios, J.D.; Fassois, S.D. A global statistical model based approach for vibration response-only damage detection under various temperatures: A proof-of-concept study. *J. Mech. Syst. Signal Process.* **2014**, *49*, 77–94.
53. Deng, L.; Duan, L.L.; He, W. Study on vehicle model for vehicle-bridge coupling vibration of highway bridge in China. *China J. Highw. Transp.* **2018**, *31*, 92–100.